運輸省港湾技術研究所

港湾技術研究所報告

REPORT OF THE PORT AND HARBOUR RESEARCH INSTITUTE

MINISTRY OF TRANSPORT

VOL. 35 NO. 1 MAR. 1996

NAGASE, YOKOSUKA, JAPAN

港湾技術研究所報告（REPORT OF P. H. R. I.）

第35巻　第1号（Vol.35, No.1），1996年３月（Mar.1996）

目　次（CONTENTS）

REPORT OF PORT AND
HARBOUR RESEARCH INSTITUTE
Vol.35, No.1 (Mar. 1996)

1. Wave Height and Fraction of Breaking Waves on a Bar-Trough Beach — Field Measurements at HORS and Modeling —

Yoshiaki KURIYAMA * and Yasushi OZAKI **

Synopsis

Field measurements of wave height and the fraction of breaking waves on longshore bars and troughs are conducted at Hazaki Oceanographical Research Station (HORS) facing the Pacific Ocean. The fraction of breaking waves decreases toward the shore on a trough, and the decrease rate depends on topographic properties of the bar; the decrease rate increases as the water depth at the bar crest decreases or as the bar height, the difference between the water depth at the trough and that at the bar crest, increases. Field data obtained on the troughs show that the wave height-water depth ratio at wave reforming decreases as the wave period decreases. Compared with the wave height-water depth ratios in a small-scale experiment, most ratios in the field are small.

Models for wave height and the fraction of breaking waves are developed; the models employ a wave-by-wave approach, where the shoaling, breaking and reforming of an individual wave are calculated. The performances of the models calibrated with experimental data are not satisfied; the fractions of breaking waves estimated by the models are smaller than the values measured on troughs. The models therefore are calibrated and verified with the field data. Furthermore, the validity of the models calibrated with the field data is confirmed with large- scale experiment data.

Key words : Fraction of breaking waves, Modeling, Field measurement, Bar-trough beach Longshore bar, Surf zone, Wave height

* Senior Research Engineer, Marine Environment Division

** Former Member of Littoral Drift Laboratory, Hydraulic Engineering Division
(Komatsujima Port Construction Office of the Third District Port Construction Bureau)

港湾技術研究所報告
第35巻第1号 (1996. 3)

1. バー型海岸における波高と砕波率の岸沖分布
—波崎海洋研究施設における現地観測とモデルの開発—

栗山善昭*・尾崎　靖**

要　旨

従来モデルでは推定精度の低かった沿岸砂州岸側のトラフ領域における砕波率の推定精度の向上を目的として，現地の沿岸砂州周辺で砕波率の観測が実施され，波高，砕波率の推定モデルが開発された。

現地観測は，鹿島灘に面する波崎海洋研究施設（HORS）で行われ、水位が超音波式波高計によって測定されるとともに，砕波，非砕波の状態が桟橋上方から目視で観察された。

トラフ領域で同時に計測された2地点の水位・砕波データを基にトラフ領域での砕波率分布と密接に関連している波の再生条件が検討された。その結果，波が再生するときの波高水深比と水深を沖波波長で無次元化した値との間に負の相関のあることが見いだされた。

続いて砂州周辺の砕波率の岸沖分布特性が調べられた。すると，砕波率のピークが砂州頂部よりも岸側となるケースが，砂州頂部での観測値のある8ケース中6ケースあった。砂州頂部よりも岸側に注目すると，砕波率の減衰は砂州の比高（トラフの水深と砂州頂部の水深との差）を砂州頂部水深で無次元化した値が大きいほど大きかった。

最後に，本観測で得られた波の再生条件を組み込んだ波浪変形シミュレーションモデルが開発され，現地データと大型水路実験データで検証された。本モデルは，現地および大型水路実験における波高，砕波率を精度良く推定することができた。

キーワード：砕波率，モデル，現地観測，バー型海岸，沿岸砂州，砕波帯，波高

* 海洋環境部　主任研究官
** 前　水工部　漂砂研究室
（現　第三港湾建設局　小松島港工事事務所）

Contents

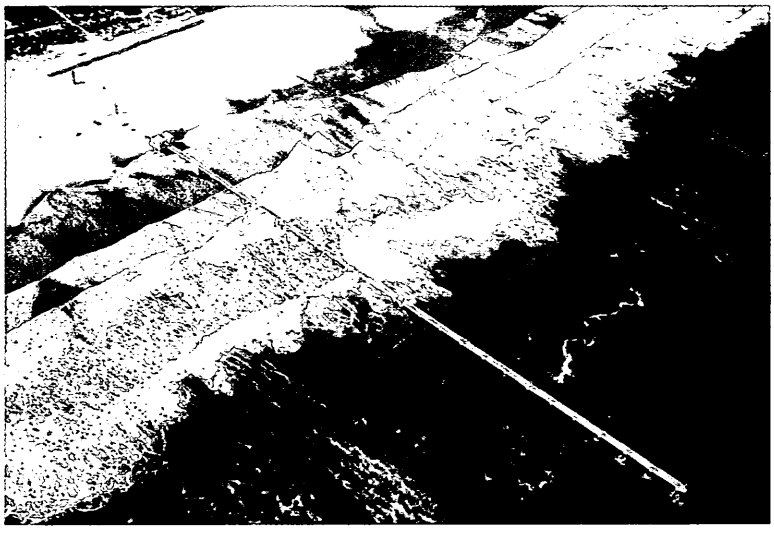

Photograph 1 Aerial view of HORS.

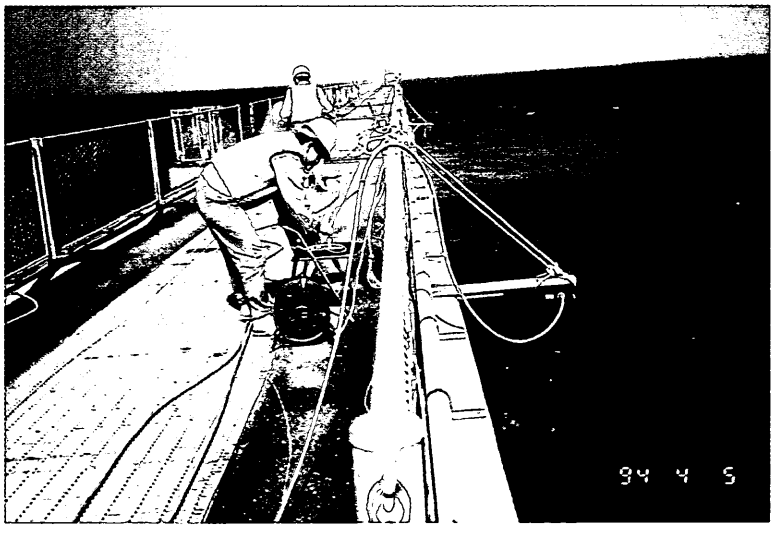

Photograph 2 Ultrasonic wave gage.

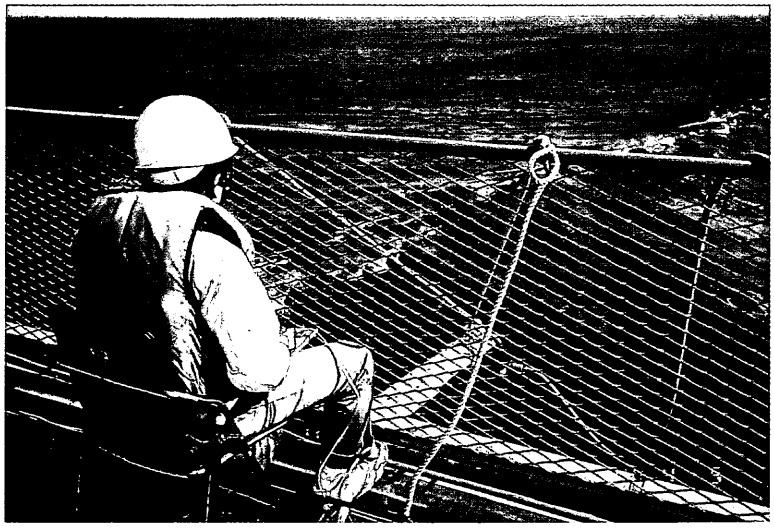

Photograph 3 Visual observation of mode of wave breaking.

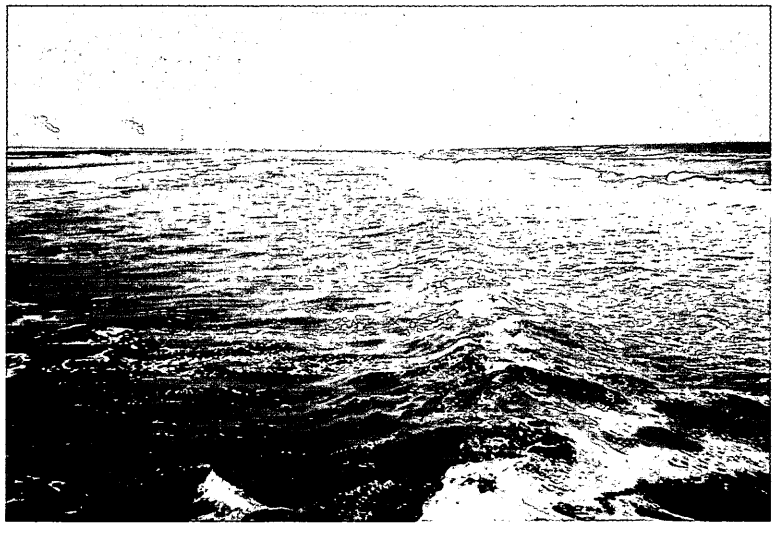

Photograph 4 Distribution of foam over a longshore bar and trough.

1. Introduction

The fraction of breaking waves, defined as the ratio of the number of breaking/broken waves to the total number of waves, is supposed to have strong effect on various phenomena in the surf zone such as nearshore current, sediment suspension, and morphology change; here, a breaking wave is defined to be in the act of breaking and a broken wave is defined to have already broken and not yet reformed. This is because various surf zone phenomena are mainly caused by turbulence, mass flux and momentum flux induced by breaking/broken waves, which are much greater than those induced by non-breaking waves. For example, *Kuriyama* (1994) carried out numerical simulations to show that the longshore current distribution over a longshore bar and trough is dependent on the cross-shore distribution of the fraction of breaking waves. Hence, to predict variations in wave height within the surf zone, as well as longshore current and undertow velocities, suspended sediment concentrations and topography changes, it is essential to accurately estimate the fraction of breaking waves Q_b.

Several models have been proposed to estimate Q_b and wave height *H. Battjes and Janssen* (1978) simulated variations in H within the surf zone, assuming a modified Rayleigh distribution truncated at the breaking wave height H_b, where breaking and broken waves have the same value of H_b. They estimated the time-averaged dissipation rate of wave energy by a periodic bore model incorporating H_b and Q_b, and Q_b was estimated by

$$\frac{1-Q_b}{-\ln Q_b}=\left(\frac{H_{rms}}{H_b}\right)^2, \tag{1}$$

where H_{rms} is the root-mean-square wave height.

Battjes and Stive (1985), *Roelvink* (1993) and *Southgate and Nairn* (1993) compared Q_b estimated by Eq.(1) with results of field measurements and experiments on planar beaches. Although the estimated values of Q_b were comparatively smaller than the measured values, the estimated cross- shore distributions of Q_b qualitatively agreed with those measured.

Thornton and Guza (1983) improved the Battjes and Janssen's model; an unmodified Rayleigh distribution, not truncated at the breaking wave height, was assumed at any location inside and outside the surf zone and wave breaking was assumed to occur at any wave height with a probability of $P_b(H)$. The time-averaged dissipation rate of wave energy was estimated by another periodic bore model, in which one equation is slightly different from that in the Battjes and Janssen's model. The value of Q_b was estimated by the following equation with a weighting function $W(H)$ and the Rayleigh wave height probability density function $p(H)$.

$$\begin{aligned} &Q_b=\int_0^\infty P_b(H)dH,\ P_b(H)=W(H)p(H),\\ &W(H)=\left(\frac{H_{rms}}{\gamma h}\right)^2\left[1-\exp\left(-\left(\frac{H}{\gamma h}\right)^2\right)\right],\quad \gamma=0.42,\\ &p(H)=\frac{2H}{H_{rms}^2}\exp\left[-\left(\frac{H}{H_{rms}}\right)^2\right]. \end{aligned} \tag{2}$$

They measured Q_b on a planar beach in the field, and found that Q_b calculated by Eq.(2) agreed well with the measured values.

Recently, *Dally* (1992) simulated variations in wave height by applying another algorithm, a wave-by-wave approach, where the shoaling, breaking and reforming of an individual wave are calculated. Because the mode of wave breaking, breaking or broken or non-breaking, of an individual wave is clarified at any point through the calculation for the individual wave, Q_b can be directly estimated as the ratio of the number of breaking/broken waves to the total number of waves. By comparing calculated results with those measured

on a longshore bar in the field by *Ebersole* (1987), Dally showed that Q_b calculated at the seaward slope of the bar had good correlation with measured values, though the calculated values were comparatively smaller than the measured values. He guessed this underestimation was due to seaward winds.

Southgate and Wallace (1994) introduced the "persistence length" into the Battjes and Janssen's model; beyond the persistence length, a broken wave reforms regardless of the wave condition. This length was assumed to be proportional to H_b, and the proportional coefficient was determined so that model results fitted to Q_b measured in large-scale experiments.

The models reviewed above predicted the cross-shore distributions of Q_b well quantitatively or at least qualitatively on planar beaches and on the seaward slopes of longshore bars. At troughs, however, the models could not predict the distributions of Q_b even qualitatively. *Rivero et al.* (1994) as well as *Southgate and Nairn* (1993) compared Q_b estimated by the Battjes and Janssen's model with those measured in experiments, and showed that the Battjes and Janssen's model considerably underestimated Q_b at troughs. Dally's model also significantly underestimated Q_b at a trough (*Dally*, 1992; *Nishi*, 1994). Although use of the "persistence length" improved the accuracy of determining Q_b at a trough (*Southgate and Wallace*, 1994), the application of their model is thought to be limited because the coefficient for calculating the persistence length was determined without physical basis; the persistence length itself was not investigated. Consequently, development of a more reliable model requires more emphasis to be directed at investigating wave reforming and the associated fraction of breaking waves at a trough.

In this study, we hence carry out field measurements of the fractions of breaking waves over longshore bars and troughs to investigate wave reforming. Then, we develop two models that can more precisely predict the cross-shore distributions of wave height and the fraction of breaking waves. The models are calibrated and verified with field and large-scale experiment data.

2. Field measurements and analysis

2.1 Field measurements

Field measurements were taken at Hazaki Oceanographical Research Station (HORS), formerly called Hazaki Oceanographical Research Facility (HORF). HORS is a field observation pier of 427 m in length at the Kashimanada-Coast facing the Pacific Ocean as shown in **Figure 1**; an aerial view of HORS is shown in **Photograph 1**.

Figure 2 shows the mean beach profile from March 1, 1994 to January 31, 1995, when the field measurements were conducted; the short vertical lines on the mean beach profile show the standard deviations in elevation based on the datum line in Hasaki, which is equal to the low water level. The offshore distance is based on a reference point located near the entrance of HORS, and is positive seaward. Any position at HORS will be referred to with the offshore distance relative to the reference point and the mark "P"; for example, P230m denotes the position where the offshore distance is 230 m. Beach profiles from P0m to P385m (the tip of HORS) were measured every 5 m with a 5 kg lead weight, while those from P-115m to P0m were measured every 5 m with a level and a staff. From March 1994 to January 1995, bars frequently formed around P200m and troughs formed around P160m.

Water surface elevations and modes of wave breaking of individual waves (breaking or broken or non-breaking) were simultaneously measured for 20 minutes at six points located over a longshore bar and trough. Water surface elevations were measured with ultrasonic wave gages installed on a side of the HORS pier deck at a sampling frequency of 2 Hz. Modes of wave breaking were visually observed. When foam was observed on a wave crest, the wave was judged to be a breaking/broken wave, and a pulse signal was manually input; the pulse signal was recorded with corresponding water surface elevation data. Due to

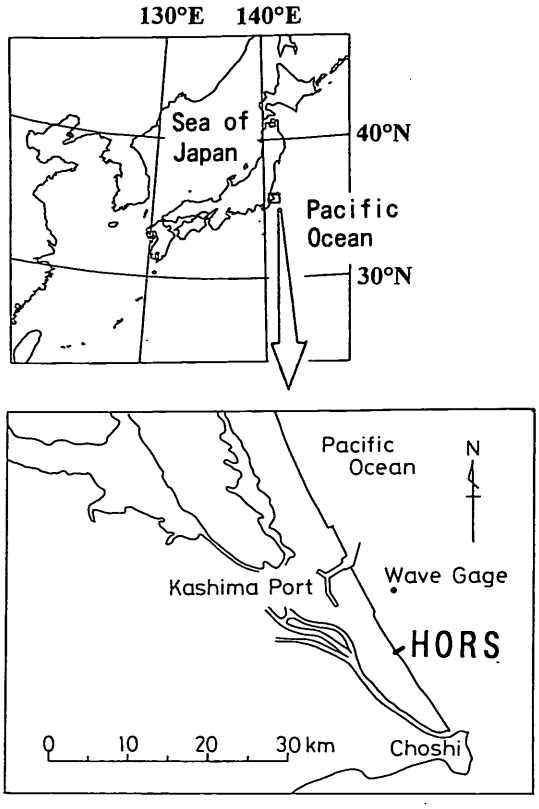

Figure 1 Investigation site.

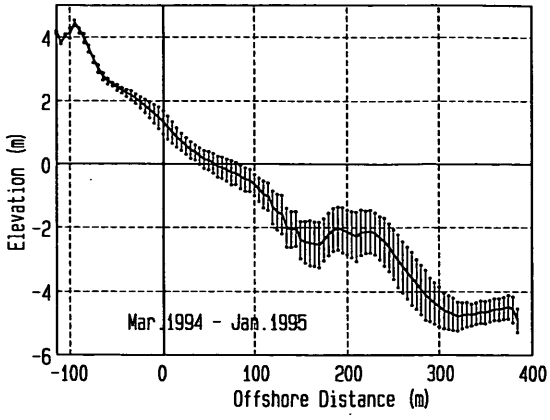

Figure 2 Mean beach profile and the standard deviations of the elevations from March 1,1994 to January 31, 1995.

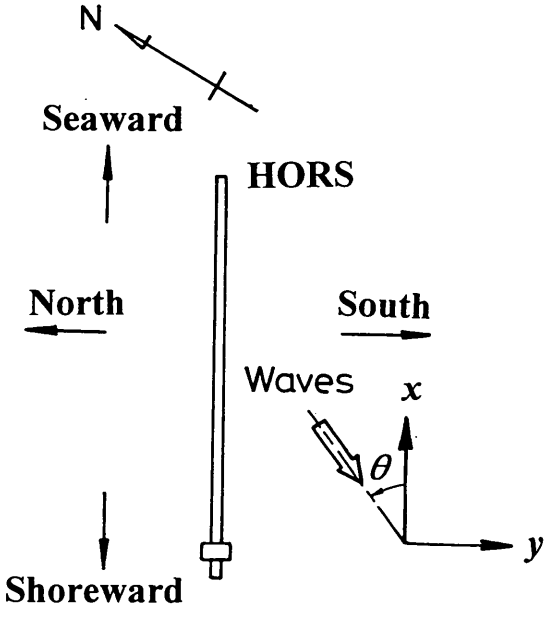

Figure 3 Definition sketch of coordinate reference system.

limited personnel availability, these measurements could only be taken at two points at a time, and accordingly, three sets of simultaneously taken measurements were required. **Photograph 2** shows an ultrasonic wave gage used in the measurements, and **Photograph 3** shows a visual observation of mode of wave breaking; the wave in **Photograph 3** was judged to be a breaking wave. **Photograph 4** shows the distribution of foam over a longshore bar and trough; the distribution of foam indicates whether breaking/broken or non-breaking waves are dominant.

Corresponding wind speeds and directions were measured with an anemometer installed at the tip of HORS (P385m), and offshore waves were measured with a wave gage located offshore the Kashima Port at 23.4 m below the Kashima datum line; the location of the gage is shown in **Figure 1**.

Figure 3 shows the employed coordinate reference system, where the x- and y-axes are positive in the seaward and southward directions, respectively. The wave direction θ is defined relative to the shoreward direction and positive counterclockwise. The vertical axis extends upward from the Hasaki datum line.

2.2 Data analysis

From water surface elevation data, the time-averaged water level assumed to be constant during a measurement is removed. To remove noise spikes, we applied a trial-and-error methodology to establish the following four criteria. The i-th water surface elevation η_i that satisfies one of the four criteria is considered to be a noise, and then the noise is replaced by a value that is linearly interpolated between the closest neighboring non-noise values. The four criteria are

a) $\eta_i > 8\eta_{rms}$, where η_{rms} is the root-mean-square value of water surface elevations,

b) $\eta_i < -7\eta_{rms}$,

c) $\eta_i - \eta_{i-1} > 4\eta_{rms}$ and $\eta_{i+1} - \eta_i < -4\eta_{rms}$,

d) $\eta_i - \eta_{i-1} < -4\eta_{rms}$ and $\eta_{i+1} - \eta_i > 4\eta_{rms}$.

After the removal of noise spikes, the resultant data are separated into high and low frequency components with the FFT (Fast Fourier Transform) method; the boundary frequency is set to be 0.04 Hz. The high frequency components are then analyzed with the zero-down crossing method. To remove extremely small waves generated by wave decomposition, we set a narrow band around zero according to *Hotta and Mizuguchi* (1980), that is, when the maximum water surface elevation in a wave does not exceed the band's upper boundary or the minimum elevation does not exceed the lower boundary, the wave is considered to be a part of the next wave. Because no theoretically based standard exists for removing small waves (*Hotta and Mizuguchi*, 1980), we set the "removal band" using the following standards:

(1) The band width W_b is determined so that the number of waves having wave height H smaller than 0.25 times the mean wave height H_m is less than that between $0.25H_m$ and $0.5H_m$.

(2) The value of H_m increases with the increase of W_b. As W_b increases, the rate of change of H_m versus W_b decreases and gradually approaches to a constant value. The value of W_b is determined so that this rate of change is close to the constant.

By applying the standards to data shoreward of bar crests, where waves frequently decompose, we determined the upper and lower boundaries of the band to be 0.3 η_{rms} and -0.3 η_{rms}. **Figure 4** shows a set of wave height distributions at a bar crest estimated with various values of W_b. The data in the figure were obtained on June 14, 1994 at P230m; the beach profile will be shown in **Figure 5 (5)**. Note that when W_b/

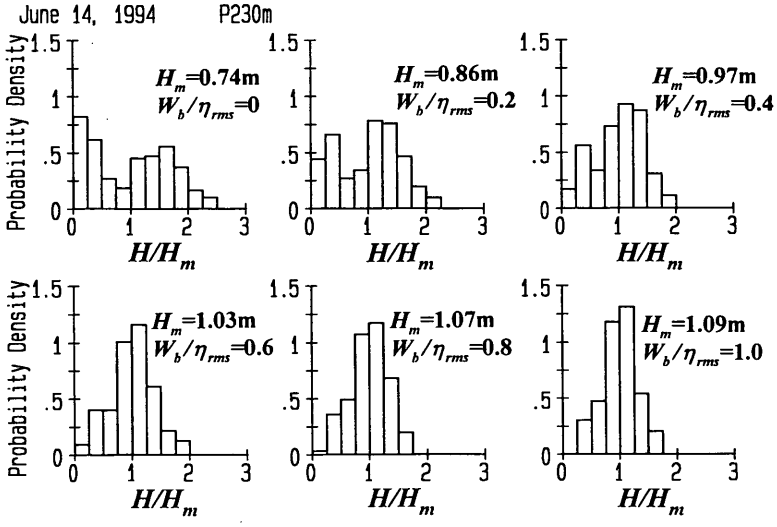

Figure 4 Wave height distributions obtained with various values of W_b.

η_{rms}=0, the number of the waves with $H < 0.25H_m$, denoted as N_{25}, is larger than that for $0.25H_m < H < 0.5H_m$, N_{50}, whereas when $W_b/\eta_{rms} > 0.2$, $N_{25} < N_{50}$. Also note that the rate of change of H_m against W_b/η_{rms} decreases as W_b/η_{rms} increases, that is, the value of H_m increases by 0.11 as W_b/η_{rms} increases from 0.2 to 0.4, while it only increases by 0.04 as W_b/η_{rms} increases from 0.6 to 0.8. Thereby this example shows that W_b= $0.6\eta_{rms}$ satisfies both standards.

When a pulse signal is included in the data set of a wave, the wave is judged as breaking/broken wave. The fraction of breaking waves is estimated as the ratio of the number of breaking/broken waves to that of all waves.

3. Fractions of breaking waves and wave heights measured on longshore bars and troughs

Eleven data sets where the maximums of Q_b were greater than 0.4 are used in the following analysis. **Table 1** lists the corresponding wave and wind conditions: the significant wave heights in deep water $(H_{1/3})_0$, the significant wave periods in deep water $(T_{1/3})_0$, the wave directions visually observed at bar crests θ_b, and the cross-shore and longshore wind velocities, W_c and W_l.

Table 1 Wave and wind conditions in the measurements

Case	Time	$(H_{1/3})_0$ (m)	$(T_{1/3})_0$ (s)	θ_b (deg.)	W_c (m/s)	W_l (m/s)
1	Mar. 3,1994,13:20-14:50	1.28	11.2	10	-3.9	-3.3
2	Mar. 10,1994,13:10-14:40	2.27	9.5	5	-8.0	7.4
3	May. 13,1994,10:20-11:45	0.95	6.2	-5	-5.6	0.1
4	June.13,1994,11:35-13:05	0.98	7.9	-20	-0.8	1.8
5	June.14,1994,13:20-14:40	1.50*	9.2	-5	-2.3	-0.4
6	June.22,1994, 9:40-11:05	1.00	7.8	15	-0.6	2.8
7	June.28,1994,13:20-14:40	1.25	5.6	20	-6.1	3.4
8	Nov. 22,1994,10:10-11:40	1.68	7.0	0	-3.2	2.4
9	Jan. 25,1995,11:00-12:30	2.37	11.1	15	1.7	6.0
10	Jan. 25,1995,14:00-15:30	2.40	11.8	15	0.4	-4.7
11	Jan. 26,1995,10:40-12:00	2.38*	13.2*	5	2.8	1.4

*obtained about three hours before the measurement

Figures 5 (1) - (11) show the corresponding cross-shore distributions of Q_b, $H_{1/3}$, and $T_{1/3}$ as well as the beach profiles, where $H_{1/3}$ and $T_{1/3}$ are the significant wave height and period. In the upper figures, the solid circles connected with solid lines show $H_{1/3}$ and the open circles connected with thin dashed lines show $T_{1/3}$. An ultrasonic wave gage did not function properly for Cases 9 - 11, and thus the associated values of Q_b are estimated as the ratios of the numbers of pulse signals to the means of the numbers of total waves measured with the normal wave gage.

Cross-shore distributions of Q_b in which Q_b shoreward of a bar crest is greater than that at the bar crest occurred in six cases (Cases 4, 5, 7, 9 ,10, and 11) out of eight cases where Q_b were measured at the bar crests; the other two cases, where these distributions did not occur, are Cases 3 and 6. A distribution like this was also observed during the Delta Flume '93 Experiment (*Rivero et al.*, 1994; *Southgate and Wallace*, 1994). A cause of this distribution is thought to be as follows. A wave undergoing wave breaking at a bar

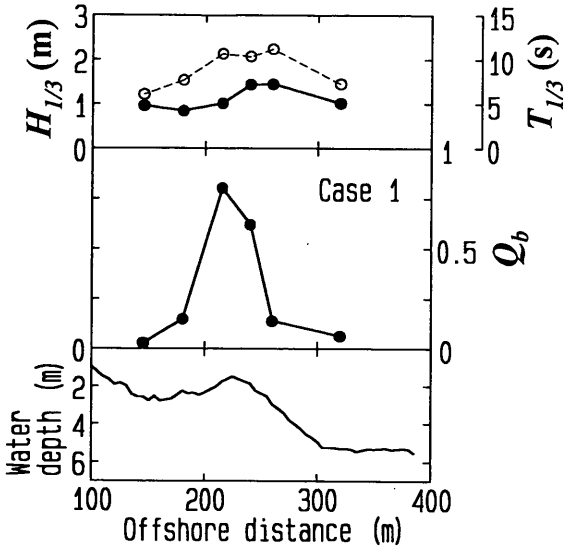

Figure 5 (1) Cross-shore distributions of $H_{1/3}$ (closed circles), $T_{1/3}$ (open circles), and Q_b, and the beach profile measured in Case 1.

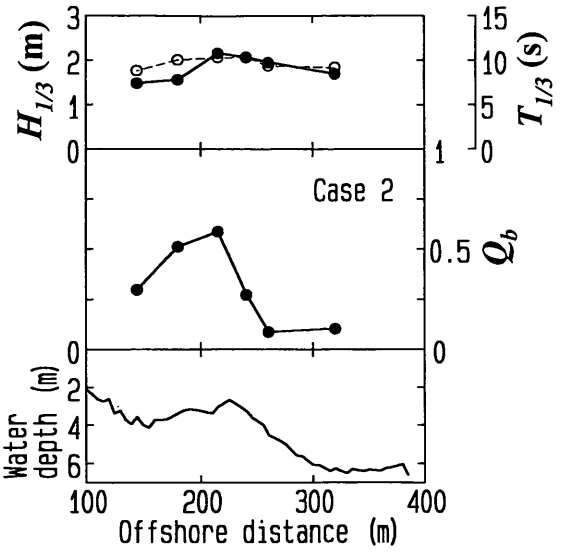

Figure 5 (2) Cross-shore distributions of $H_{1/3}$ (closed circles), $T_{1/3}$ (open circles), and Q_b, and the beach profile measured in Case 2.

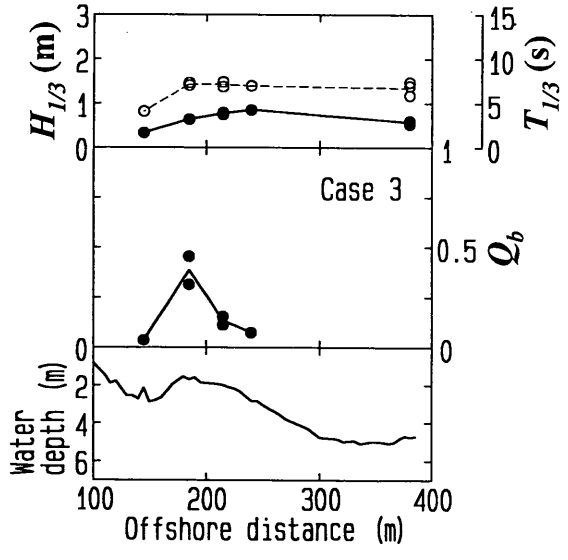

Figure 5 (3) Cross-shore distributions of $H_{1/3}$ (closed circles), $T_{1/3}$ (open circles), and Q_b, and the beach profile measured in Case 3.

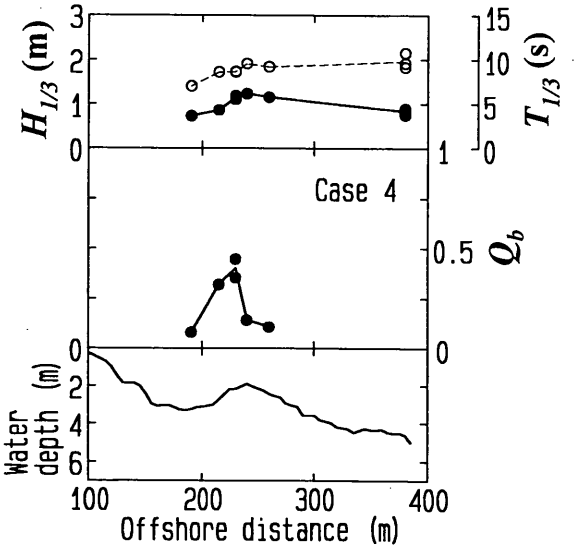

Figure 5 (4) Cross-shore distributions of $H_{1/3}$ (closed circles), $T_{1/3}$ (open circles), and Q_b, and the beach profile measured in Case 4.

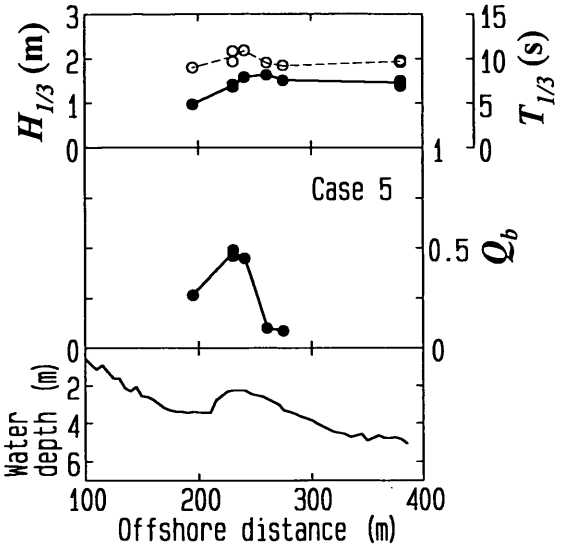

Figure 5 (5) Cross-shore distributions of $H_{1/3}$ (closed circles), $T_{1/3}$ (open circles), and Q_b, and the beach profile measured in Case 5.

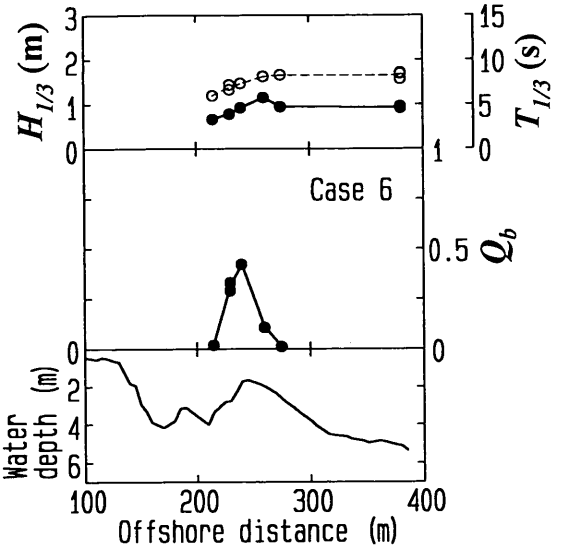

Figure 5 (6) Cross-shore distributions of $H_{1/3}$ (closed circles), $T_{1/3}$ (open circles), and Q_b, and the beach profile measured in Case 6.

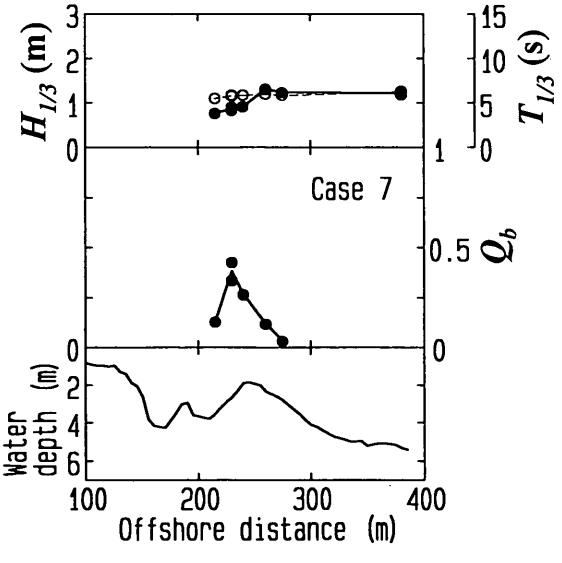

Figure 5 (7) Cross-shore distributions of $H_{1/3}$ (closed circles), $T_{1/3}$ (open circles), and Q_b, and the beach profile measured in Case 7.

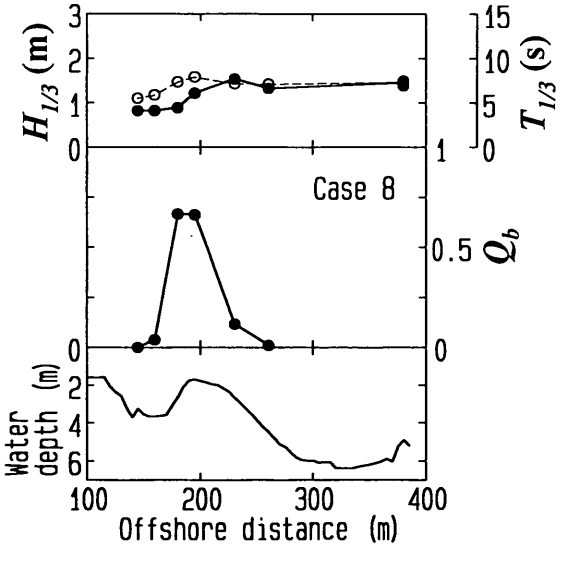

Figure 5 (8) Cross-shore distributions of $H_{1/3}$ (closed circles), $T_{1/3}$ (open circles), and Q_b, and the beach profile measured in Case 8.

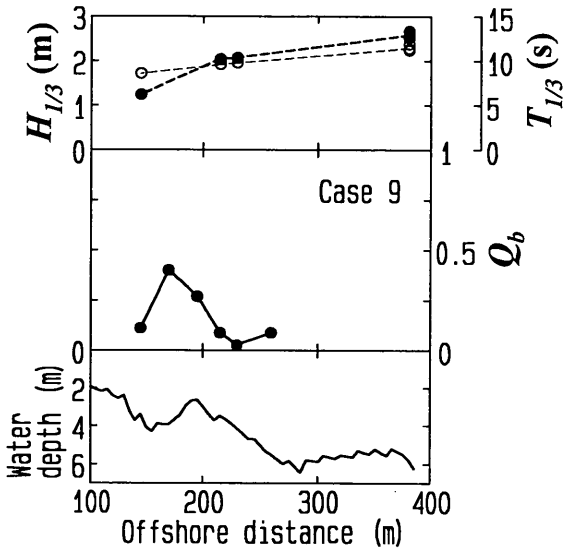

Figure 5 (9) Cross-shore distributions of $H_{1/3}$ (closed circles), $T_{1/3}$ (open circles), and Q_b, and the beach profile measured in Case 9.

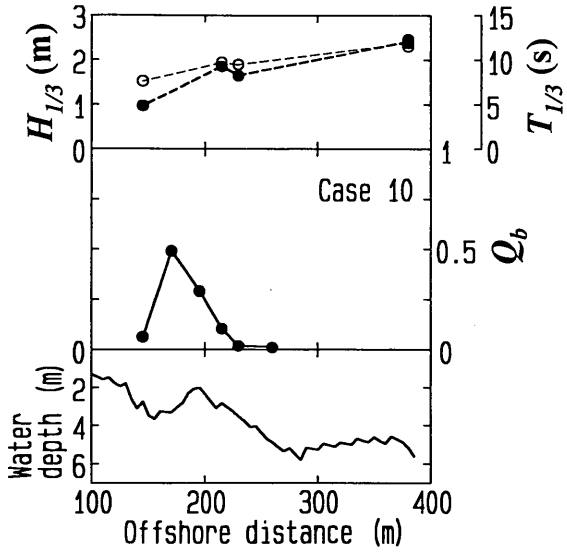

Figure 5 (10) Cross-shore distributions of $H_{1/3}$ (closed circles), $T_{1/3}$ (open circles), and Q_b, and the beach profile measured in Case 10.

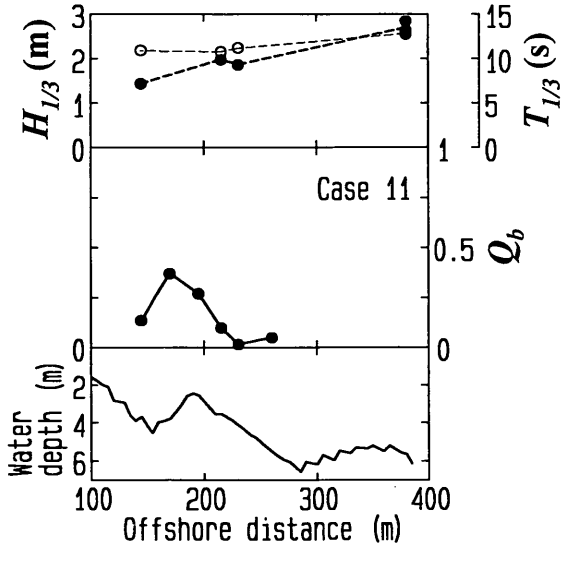

Figure 5 (11) Cross-shore distributions of $H_{1/3}$ (closed circles), $T_{1/3}$ (open circles), and Q_b, and the beach profile measured in Case 11.

crest starts to overturn so that the overturned crest plunges shoreward of the bar crest. Although this wave is counted as a breaking/broken wave shoreward of the bar crest, it is counted as a non- breaking wave at the bar crest. As a result, Q_b shoreward of the bar crest is greater than that at the crest.

Whitford and Thornton (1988) observed in the field that Q_b decreased toward a bar crest on the seaward slope of the crest. Such distribution of Q_b, however, was not observed here.

Even though the profiles of longshore bars and troughs are similar, the distributions of Q_b shoreward of the bar crests are different. For example, the profile of the longshore bar in Case 1 (**Figure 5 (1)**) is similar to that in Case 2 (**Figures 5 (2)**), yet their Q_b distributions are different; the measurements in Case 2 were conducted 7 days after the measurements in Case 1. Although the distributions of Q_b in Cases 1 and 2 have peaks at P215m, Q_b shoreward of the bar crest in Case 2 decreases gradually toward the shore, whereas in Case 1, it decreases sharply.

Consequently, we investigate the decrease of Q_b shoreward of a bar crest using a parameter containing the water depth at the bar crest h_{bar} and that at the trough h_{trg} ; Q_b shoreward of a bar crest is denoted as $(Q_b)_{shb}$. In this investigation, $(Q_b)_{shb}$ is assumed to decrease from the bar crest toward the shore proportionally to the offshore distance from the bar crest. If we define Q_b at a bar crest as $(Q_b)_{bar}$, the offshore distance as x, and the offshore distance at the bar crest as x_{bar}, then $(Q_b)_{shb}$ can be assumed that

$$(Q_b)_{shb} = A(x - x_{bar}) + (Q_b)_{bar}, \tag{3}$$

where A is a dissipation coefficient. The coefficient A is investigated with $(h_{trg} - h_{bar})/h_{bar}$, and the relation between them is shown in **Figure 6**. Note that there is a positive correlation between A and $(h_{trg} - h_{bar})/h_{bar}$, that is, A increases as $(h_{trg} - h_{bar})/h_{bar}$ increases. The reasons for this correlation are discussed in the chapter 6.

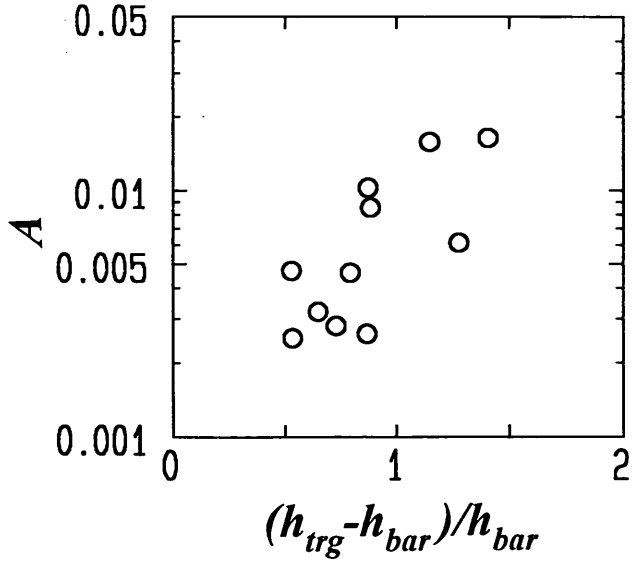

Figure 6 Relation between A and $(h_{trg} - h_{bar})/h_{bar}$.

4. Wave condition at wave reforming

For investigating the wave condition at wave reforming, the following field data are required: individual wave height H_r and period T_r, and water depth h_r at wave reforming. Those data, however, are very difficult

to obtain in the field, and hence, we estimate those values using the data of waves that are breaking/broken at the seaward measurement points and non-breaking at the shoreward measurement points. It is therefore essential to collect the sea/shoreward data of the same wave. This is done by first extracting a sequence of water surface elevations of a wave measured at a seaward point, and then extracting such elevations measured at the shoreward point that are thought to be from the same wave. Next, a correlation coefficient between the seaward and shoreward extracted data sets is calculated, and the both data sets are judged to belong to the same wave when the calculated correlation coefficient is greater than 0.85. A detailed description of this procedure is as follows.

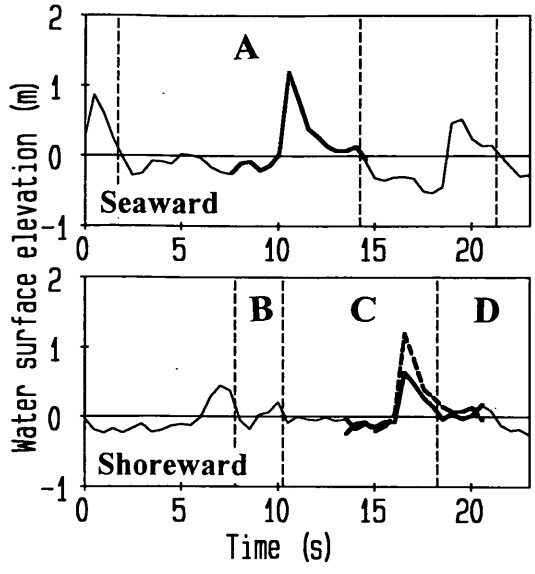

Figure 7 Example of seaward (upper figure) and shoreward (lower figure) data of water surface elevation obtained simultaneously. The wave "C" is recognized to be identical to the wave "A".

a) The extracted seaward water surface elevations of a wave are a sequence of elevations starting from the minimum elevation preceding the maximum elevation in the wave and ending at the first minus elevation after the maximum. **Figure 7** shows an example of seaward and shoreward water surface elevation data simultaneously obtained; the vertical dashed lines indicate the zero-down crossing points. Here, let us focus on the wave "A" measured at the seaward point. The extracted data of the wave "A" are shown by the bold line in the upper figure.

b) Next, several sets of shoreward data having various time lags behind the extracted seaward data are extracted; the number of the extracted shoreward data points in each set is equal to that of the extracted seaward data. The time lags are from T_l - 3 s to T_l + 3 s at 0.5 s intervals (13 sets); T_l is the period in which a wave with the mean wave period travels from the seaward point to the shoreward point. Even though an individual wave period is different from the mean wave period, T_l can still be used because field measurements of *Thornton and Guza* (1982) show that wave celerities in the surf zone are nearly independent of wave period.

c) The correlation coefficients between the extracted seaward and shoreward data are calculated, and if the maximum correlation coefficient is greater than 0.85, then the shoreward data set having the maximum coefficient is judged to belong to the same wave as the extracted seaward data set. If the extracted shoreward data belong to more than two waves, the wave having the maximum elevation in the extracted shoreward data is designated to be identical to the seaward wave. In the lower figure of **Figure 7**, the shoreward data set having the maximum correlation coefficient, 0.96, is indicated by the bold solid line, and the extracted seaward data set superimposed on it is indicated by the bold dashed line. Thus, the shoreward wave "C" is designated to be identical to the seaward wave "A".

To investigate the wave condition at wave reforming, we analyze data sets of waves that were breaking or broken at seaward points and non- breaking at shoreward points. The values of H_r and h_r are estimated as the means of the values at the seaward and shoreward points, and L_0 is estimated using the mean of the wave periods at the seaward and shoreward points. In estimating h_r, the time-averaged water levels of the high and low frequency components are considered.

The parameters of h_r/L_0 and cross-shore wind speed W_c, which is shown to influence wave breaking in

the field by *Galloway et al.* (1989) and *Dally* (1992), are used to investigate the wave height-water depth ratio at wave reforming H_r/h_r. We assume the following three relations among H_r/h_r, h_r/L_0 and $W_c/\sqrt{gh_r}$, and then calculate the Akaike's Information Criterion (AIC), which have been developed to determine the best model fitting specific data; the model with the minimum AIC value is judged to be the best one. In the field of coastal engineering, the AIC was used, for example, by *Hashimoto et al.* (1994) for estimating directional wave spectra. The AIC of a model applied to N_A data points, denoted as *AIC*, is expressed as

$$AIC = N_A \ln 2\pi + 1 + N_A \ln \sigma^2 + 2(M_A + 2), \tag{4}$$

where σ^2 is the error mean square, and M_A is the number of the free parameters contained in the model. The value of σ^2 can be estimated by

$$\sigma^2 = \frac{1}{N_A} \sum_{j=1}^{N_A} \left((H_r / h_r)_{p,j} - (H_r / h_r)_{m,j} \right)^2, \tag{5}$$

where subscripts p and m denote predicted and measured values.

The assumed three relations among H_r/h_r, h_r/L_0 and $W_c/\sqrt{gh_r}$ are as follows:

$$H_r / h_r = a_0, \tag{6}$$

$$H_r / h_r = a_0 + a_1 h_r / L_0, \tag{7}$$

$$H_r / h_r = a_0 + a_1 h_r / L_0 + a_2 W_c / \sqrt{gh_r}, \tag{8}$$

where a_0, a_1, and a_2 are dimensionless coefficients; the values of M_A in Eqs.(6), (7) and (8) are 2, 3 and 4, respectively. **Table 2** gives the calculated *AIC* and coefficient values, and shows that Eq.(7) is most suitable to express H_r/h_r.

Table 2 The values of *AIC* and the coefficient in Eqs.(6), (7), and (8)

Model	*AIC*	a_0	a_1	a_2
Eq.(6)	-339.5	0.352	—	—
Eq.(7)	-374.7	0.142	-0.0624	—
Eq.(8)	-374.3	0.157	-0.0599	0.0145

The relation between H_r/h_r and h_r/L_0 is shown in **Figure 8**, where the straight solid line represents

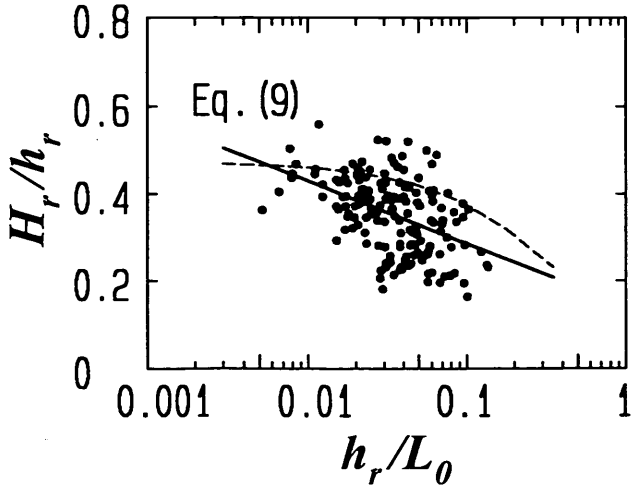

Figure 8 Relation between H_r/h_r and h_r/L_0.

Eq.(7), that is,

$$H_r / h_r = -0.0624 \ln (h_r / L_0) + 0.142 . \tag{9}$$

The dashed line in the figure is the experimentally determined criterion of wave reforming proposed by *Kweon and Goda* (1994). Compared with the experimental criterion, most H_r/h_r in the field were small.

5. Models for wave height and the fraction of breaking waves

5.1 Formulation of models

Two models developed here for predicting wave height and the fraction of breaking waves employ a wave-by-wave approach as *Dally* (1992) did; the shoaling, breaking and reforming of individual waves are calculated. The values of $H_{1/3}$ and Q_b are estimated with the simulation results of individual waves. The only difference between these models is the estimation of wave energy dissipation due to wave breaking; that is, one model, called Model 1, contains a periodic bore dissipation sub-model used by *Thornton and Guza* (1983), while the other model, called Model 2, uses a dissipation sub- model developed by *Dally et al.* (1985), in which stable wave height is included.

(1) Model 1

Shoaling of a wave is calculated with a shoaling coefficient proposed by *Shuto* (1974); the coefficient has been derived under the consideration of wave nonlinearity.

As a criterion on wave breaking, we use formulae proposed by *Seyama and Kimura* (1988), who experimentally investigated the wave height-water depth ratio at wave breaking H_b/h_b of individual irregular waves as a function of the beach slope $\tan\beta$ and the ratio of breaking water depth to the offshore wavelength h_b/L_0. They also investigated the standard deviation δ of H_b/h_b. The relation between H_b/h_b versus $\tan\beta$ and h_b/L_0, and δ are determined as

$$\frac{H_b}{h_b} = 0.16 \frac{L_0}{h_b}\left[1 - \exp\left\{-0.8\pi \frac{h_b}{L_0}\left(1 + 15\tan^{4/3}\beta\right)\right\}\right] - 0.96\tan\beta + 0.2 , \tag{10}$$

$$\delta = 0.08 H_b / h_b . \tag{11}$$

In the Model 1, the values of H_b/h_b are assumed to distribute around Eq.(10) with a normal distribution having the standard deviation estimated by Eq.(11).

After wave breaking, the energy dissipation of a wave is evaluated with its frequency f, energy E_w and group velocity C_g using

$$\frac{\partial (E_w C_g)}{\partial x} = \frac{1}{4}\rho g f \frac{(BH)^3}{h} , \tag{12}$$

where ρ is the density of sea water, g is the acceleration of gravity, and B is a dimensionless coefficient.

Thornton and Guza (1983) used Eq.(12) to calculate the total wave energy dissipation applying the same value of B to all waves, which have different wave heights. By comparing H_{rms} measured in the field and those estimated by Eq.(12), they determined B=1.5. We, however, will predict variations in H of individual waves, for which B=1.5 has not been proved to be optimum. The optimum B for individual waves is therefore investigated with experimental results shown by *Seyama and Kimura* (1988). They experimentally investigated variations in H of individual waves in the surf zone, and reported that the variations consist of three phases: an increase in H immediately after wave breaking, a sharp decrease in H after reaching the maximum wave height and a moderate decrease in H from the middle of the surf zone to

the shoreline. The corresponding formulae representing these phases, proposed by *Seyama and Kimura* (1988), are utilized for obtaining the optimum B. However, because *Seyama and Kimura* (1988) defined wave breaking differently than its definition in the Model 1, where wave breaking point is defined as the point where the maximum wave height occurs, we slightly modified their formulae so that the maximum wave height occurs at the wave breaking point. The modified formula is given by

$$\begin{aligned} H / H_b &= c_1 (h / h_b) + c_2, \quad h / h_b \geq c_3, \\ H / H_b &= c_4 (h / h_b) + c_5, \quad h / h_b < c_3, \end{aligned} \tag{13}$$

where h is the water depth, and h_b is the breaking water depth. The values of coefficients c_1 - c_5 are listed in **Table 3**.

Table 3 The values of the coefficients in Eq.(13)

$\tan\beta$	c_1	c_2	c_3	c_4	c_5
1/10	0.977	0.0242	0.444	0.988	0.0186
1/20	1.248	-0.249	0.641	0.829	0.0192
1/30	1.397	-0.396	0.706	0.807	0.0195
1/50	1.556	-0.550	0.759	0.803	0.0200

We optimize B using four waves (H_0/L_0 = 0.005, 0.01, 0.025 and 0.05) on four beach slopes ($\tan\beta$ = 1/10, 1/20, 1/30, and 1/50) so that wave heights estimated by Eq.(12) agree with those estimated by Eq.(13). The optimum B obtained is

$$B = 1.6 - 0.12 \ln (H_0 / L_0) + 0.28 \ln (\tan \beta). \tag{14}$$

Figures 9 (1) - (3) show examples of wave heights estimated by Eq.(13) and by Eq.(12) with the optimum B (Eq.(14)). The thick solid lines show wave heights estimated by Eq.(13), and the thin solid lines and the dashed lines show those estimated by Eq.(12) at H_0/L_0 = 0.005 and 0.07, respectively. Note that the Model 1 predicts variation in H well on planar beaches.

The Model 1 is also verified against experimental data of wave decay on a flat bed (*Kweon and Goda*, 1994). **Figures 10** shows comparisons of wave heights estimated by Eq.(12) and those measured at H_0/L_0 from 0.006 to 0.07; the solid circles are the measured values and the solid lines are the estimated values. Although there are some discrepancies, the Model 1 is suitable for predicting the wave decay on a flat bed.

While wave reforming is judged on the basis of Eq.(9), a random distribution is assumed at Eq.(9) - 0.2 < H_r/h_r < Eq.(9) + 0.2 due to data scatter in this region as shown in **Figure 8**.

In the Model 1, we set a certain region where a broken wave does not reform even though the wave height-water depth is less than that estimated by Eq.(9) because of the following reason. After wave breaking, a bore gradually develops on the front of a broken wave. Bore development appears to be strongly influenced by the wave condition at the wave breaking point, whereas it appears to be only slightly influenced by the wave condition shoreward of the wave breaking point. Consequently, even though $H < H_r$, the bore under development is supposed to advance toward the shore without vanishing.

We set the length of this region l based on experimental data of *Seyama and Kimura* (1988), and assume that l is equal to the distance between the point of the maximum wave height and that where a change occurs in the rate of decrease of H/H_b versus h/h_b. We suppose that bore development ends at the latter point because *Seyama and Kimura* (1988) reported the appearance of stable bores at the latter point. The length of l is accordingly expressed as

$$l = \frac{h_b}{\tan\beta}\left\{1 - 0.93\exp\left(-9.21\tan\beta\right) - \frac{0.02}{0.72\exp\left(6.11\tan\beta\right)}\right\}. \tag{15}$$

The region set in our model seems to equal the persistence length proposed by *Southgate and Wallace* (1994). However, these are slightly different; that is, we assume that a broken wave cannot reform if $H>H_r$, regardless of wave position, whereas they assume that a broken wave must reform beyond the persistence length, regardless of wave condition.

Naturally, wave shoaling is calculated again after wave reforming.

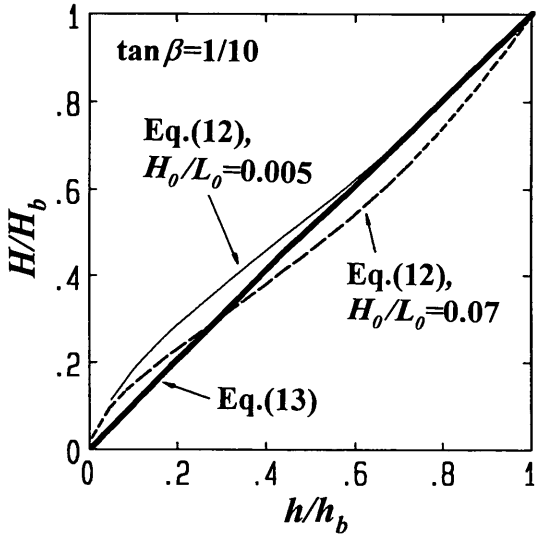

Figure 9 (1) Comparison of H/H_b estimated by Eq.(13) and Eq.(12) at $\tan\beta=1/10$.

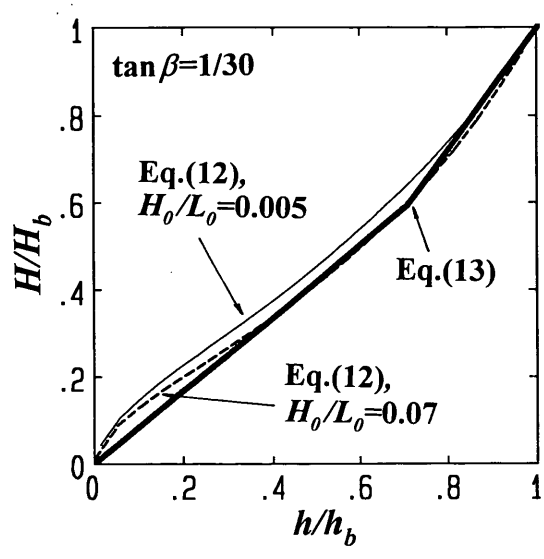

Figure 9 (2) Comparison of H/H_b estimated by Eq.(13) and Eq.(12) at $\tan\beta=1/30$.

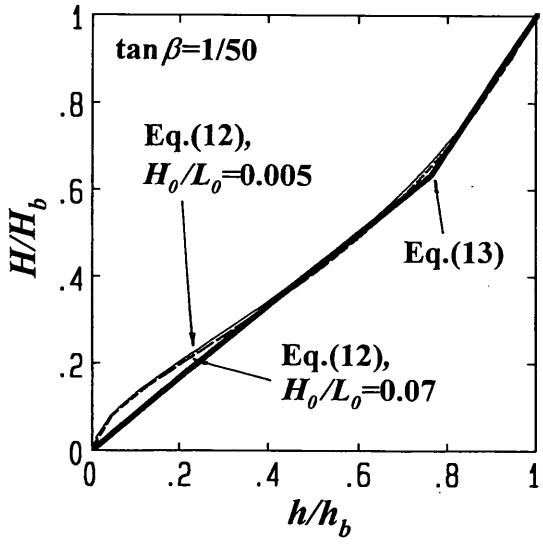

Figure 9 (3) Comparison of H/H_b estimated by Eq.(13) and Eq.(12) at $\tan\beta=1/50$.

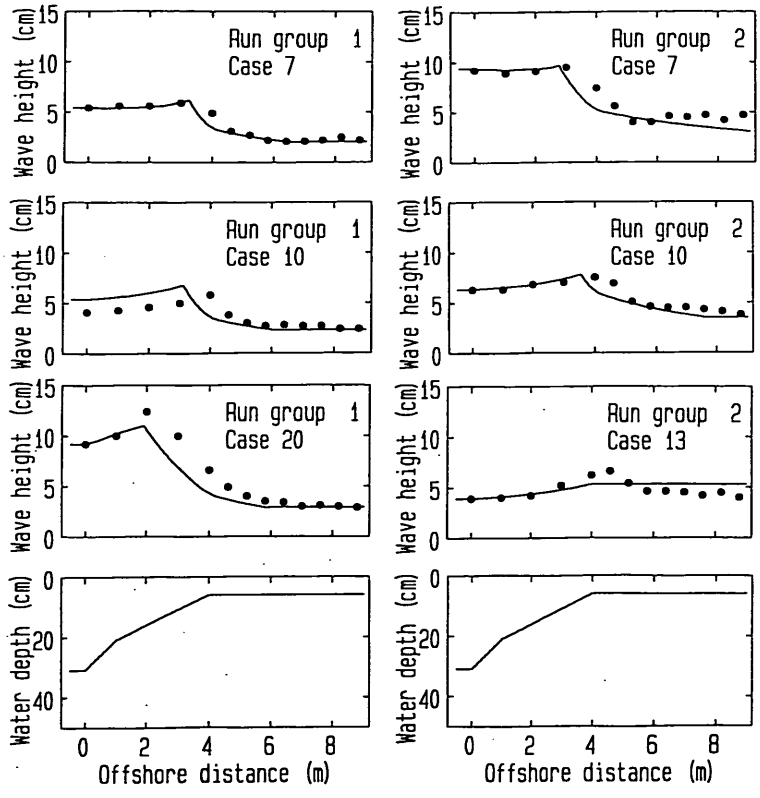

Figure 10 Comparison of wave heights on a flat bed measured in an experiment (solid circles) and estimated by Eq.(12) (solid lines).

(2) Model 2

Because the Model 2 uses the same method as that in the Model 1 to calculate shoaling, wave breaking and wave reforming of an individual wave, we only describe the method for estimating the wave energy dissipation due to wave breaking.

The wave energy dissipation is estimated by the following equation, proposed by *Dally et al.* (1985),

$$\frac{\partial (E_w C_g)}{\partial x} = (E_w C_g - E_S C_g)\frac{K}{h}, \qquad E_S = \rho g H_S^2 / 8, \; H_S = \Gamma h, \tag{16}$$

where K and Γ are dimensionless coefficients, and H_S represents the stable wave height, defined as the value of H at which wave breaking ends on a shelf beach composed of a upward sloping bottom and a flat bottom. *Dally et al.* (1985) showed that use of $K = 0.15$ and $\Gamma = 0.4$ could estimate H in good agreement with experimental data by *Horikawa and Kuo* (1966).

Since H_S represents the height of a stable wave, which is non-breaking after reforming, Γ can be considered as the wave height-water depth ratio at wave reforming. In this model, hence, Γ is replaced by a value estimated by Eq.(9), while $K = 0.15$ is maintained.

5.2 Calibration

The values of $H_{1/3}$ and Q_b for Cases 1 - 11 are estimated by the Model 1 and the Model 2, and are compared with the field data. The input wave data at the offshore boundaries, which are the wave heights

and periods of individual waves, are obtained on the basis of the field data. With the exception of Cases 9 - 11, the offshore boundaries are set at the most seaward measurement points, which are P320m in Cases 1 and 2, and P380m in Cases 3 - 8.

In Cases 1 and 2, we obtain the input wave data at the offshore boundaries, P320m, by adjusting the band width, which is discussed in 2.2, to minimize errors caused by the change of the numbers of the waves. The present models assume that the numbers of waves are constant; this means that wave periods are assumed to be constant. The values of $T_{1/3}$ measured, however, change over longshore bars and troughs as shown in **Figures 5 (1) - (11)**; $T_{1/3}$ seaward of the bar crests increase toward the crests, and then decrease shoreward of the crests in particular in Cases 1 and 2. In Cases 1 and 2, the wave periods at P320m are smaller than the means of $T_{1/3}$ measured over the longshore bars and troughs; that is, the numbers of the waves at P320m are larger than the means of the numbers over the longshore bars and troughs. Hence, the band widths are adjusted so that the numbers of the waves at P320m are equal to the mean numbers of the waves seaward of the bar crests, at P320m, P260m, and P240m, and the input wave data are obtained.

In Cases 9 - 11, the offshore boundaries are set at P230m, where Q_b were low, because of the following reason. The most seaward measurement points in Cases 9 - 11, P380m, were included in the primary surf zones, and some of the waves were broken there. However, the modes of wave breaking of the individual waves were unknown at P380m because Q_b measurements were not conducted, whereas in the calculations, judgements of wave breaking and wave reforming are essential. The offshore boundaries in Cases 9 - 11 are hence set at P230m, where few waves were broken and all individual waves can be set as non-breaking. Supplementary simple visual observations confirmed that the offshore boundaries in Cases 1 - 8 were not included in the surf zones, and therefore all individual waves at the offshore boundaries are set as non-breaking.

Figures 11 (1) - (11) show comparisons of $H_{1/3}$ and Q_b measured in the field (solid circles) and those estimated by the Model 1 (thick solid lines) and the Model 2 (thin dashed lines). Good agreements exist between the models for Q_b and $H_{1/3}$. The values of Q_b estimated by the Model 1 and the Model 2, however, are considerably smaller than the measured values on the troughs, and are also smaller than the measured values even on the seaward slopes of the longshore bars. Furthermore, the values of $H_{1/3}$ estimated by the Model 1 and the Model 2 are smaller than the measured values on the troughs. These results show that waves in the models tend to break less and decay more than waves in the field. We think the tendency of the waves in the models is due to scale effect; all coefficients in the models expect for those of the wave reforming criterion were determined on the basis of experimental data. Hence, we introduce new coefficients and calibrate the models with the field data.

Instead of Eq.(10), which is the criterion of wave breaking in the Model 1 and the Model 2, the following equation with a dimensionless coefficient C_{br} is introduced.

$$\frac{H_b}{h_b} = C_{br}\left(0.16\frac{L_0}{h_b}\left[1-\exp\left\{-0.8\,\pi\frac{h_b}{L_0}\left(1+15\tan^{4/3}\beta\right)\right\}\right]-0.96\tan\beta+0.2\right). \tag{17}$$

Equation (14), which is used for the calculation of wave energy dissipation in the Model 1, is replaced by

$$B = C_B\left\{1.6-0.12\ln\left(H_0/L_0\right)+0.28\ln\left(\tan\beta\right)\right\}, \tag{18}$$

where C_B is a new dimensionless coefficient.

The calibrations for the Model 1 are conducted by varying the values of C_{br} and C_B, and by determining the optimum values that minimize errors between predicted and measured values of $H_{1/3}$ ad Q_b, while the

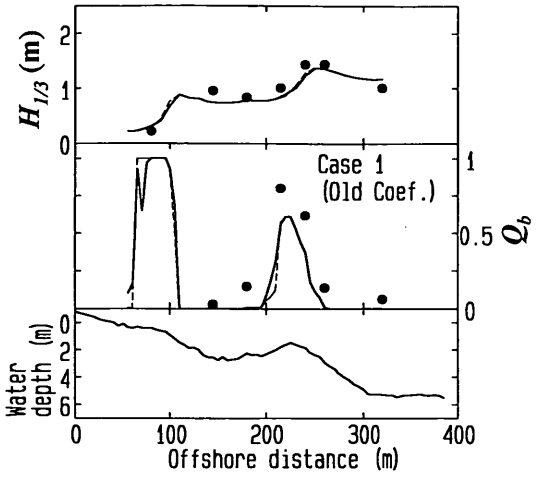

Figure 11 (1) Comparison of $H_{1/3}$ and Q_b measured in the field (solid circles) and those estimated by the Model 1 (thick solid lines) and the Model 2 (thin dashed lines) in Case 1.

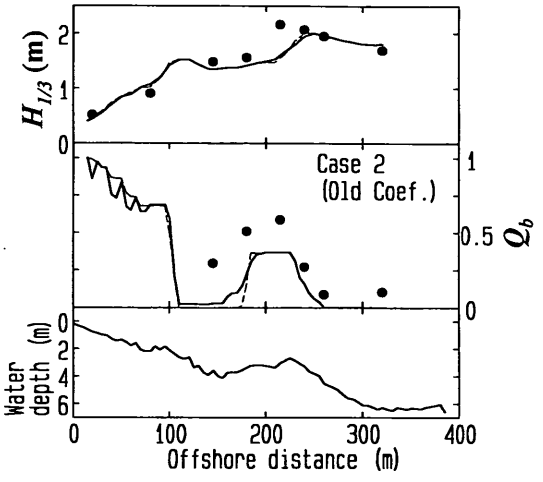

Figure 11 (2) Comparison of $H_{1/3}$ and Q_b measured in the field (solid circles) and those estimated by the Model 1 (thick solid lines) and the Model 2 (thin dashed lines) in Case 2.

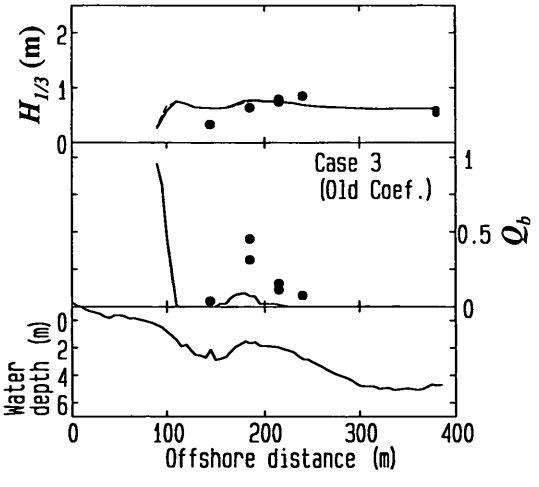

Figure 11 (3) Comparison of $H_{1/3}$ and Q_b measured in the field (solid circles) and those estimated by the Model 1 (thick solid lines) and the Model 2 (thin dashed lines) in Case 3.

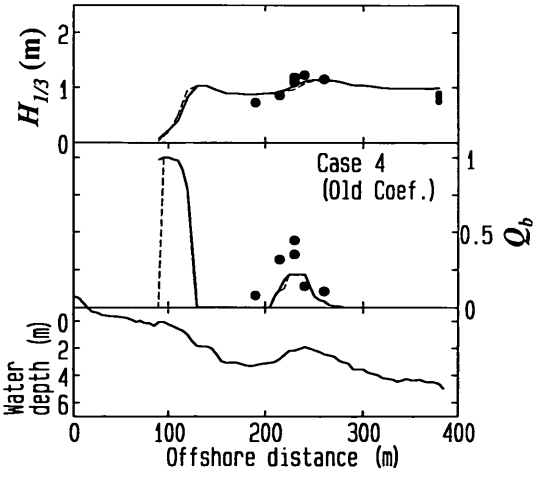

Figure 11 (4) Comparison of $H_{1/3}$ and Q_b measured in the field (solid circles) and those estimated by the Model 1 (thick solid lines) and the Model 2 (thin dashed lines) in Case 4.

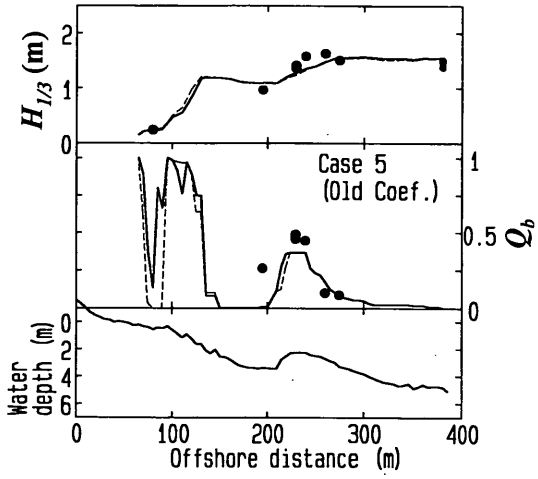

Figure 11 (5) Comparison of $H_{1/3}$ and Q_b measured in the field (solid circles) and those estimated by the Model 1 (thick solid lines) and the Model 2 (thin dashed lines) in Case 5.

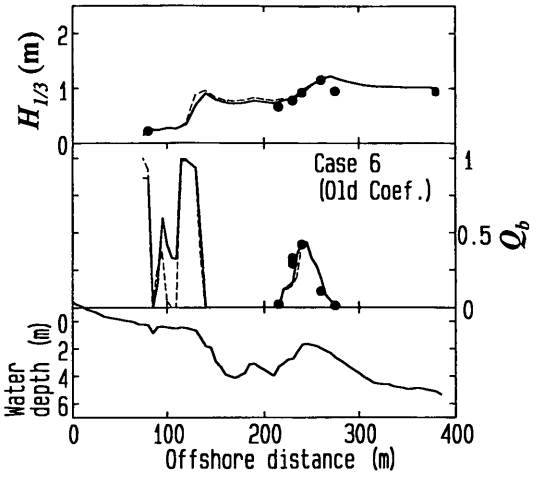

Figure 11 (6) Comparison of $H_{1/3}$ and Q_b measured in the field (solid circles) and those estimated by the Model 1 (thick solid lines) and the Model 2 (thin dashed lines) in Case 6.

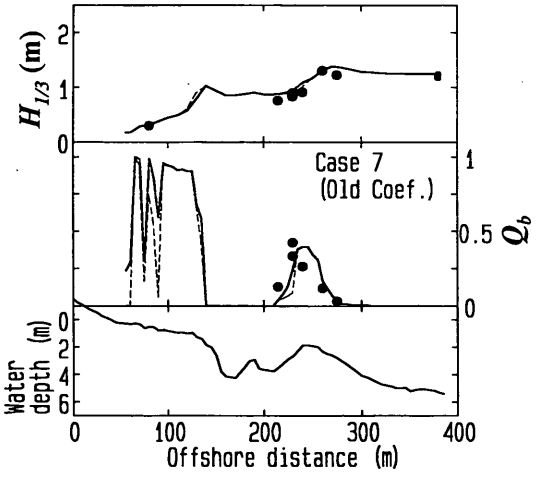

Figure 11 (7) Comparison of $H_{1/3}$ and Q_b measured in the field (solid circles) and those estimated by the Model 1 (thick solid lines) and the Model 2 (thin dashed lines) in Case 7.

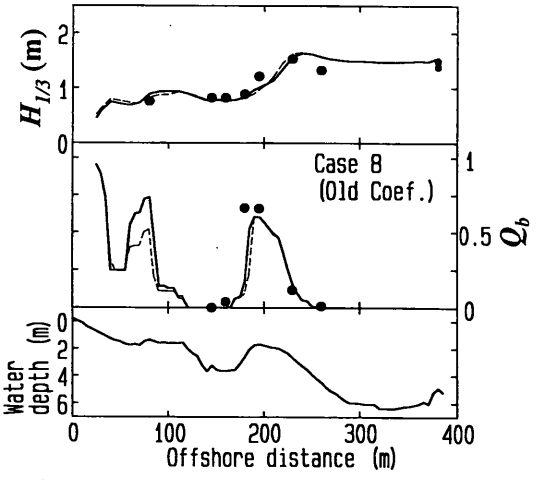

Figure 11 (8) Comparison of $H_{1/3}$ and Q_b measured in the field (solid circles) and those estimated by the Model 1 (thick solid lines) and the Model 2 (thin dashed lines) in Case 8.

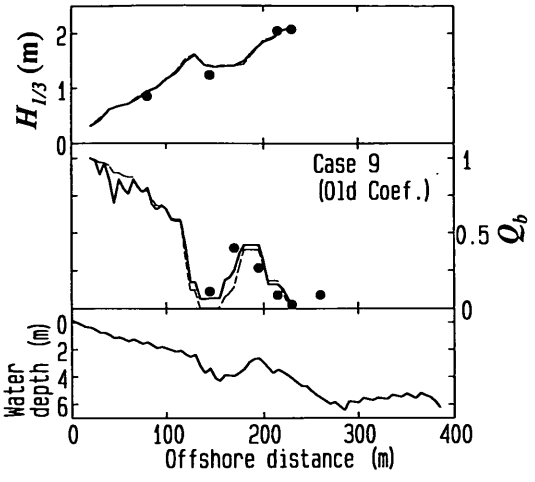

Figure 11 (9) Comparison of $H_{1/3}$ and Q_b measured in the field (solid circles) and those estimated by the Model 1 (thick solid lines) and the Model 2 (thin dashed lines) in Case 9.

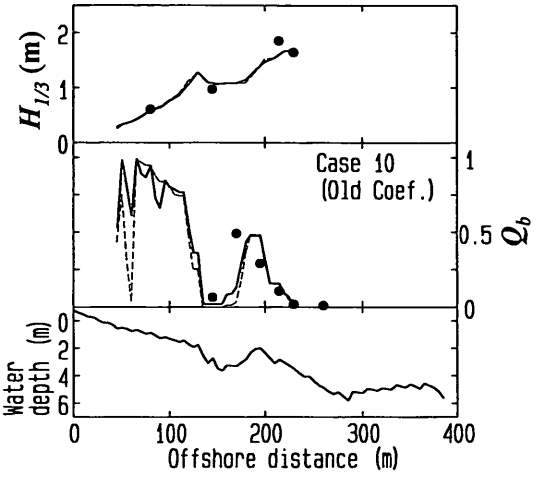

Figure 11 (10) Comparison of $H_{1/3}$ and Q_b measured in the field (solid circles) and those estimated by the Model 1 (thick solid lines) and the Model 2 (thin dashed lines) in Case 10.

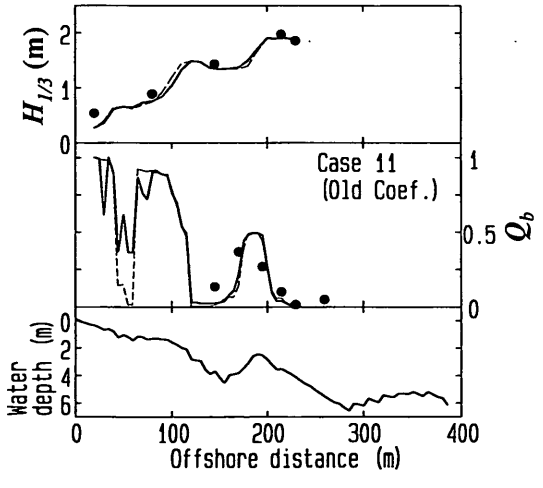

Figure 11 (11) Comparison of $H_{1/3}$ and Q_b measured in the field (solid circles) and those estimated by the Model 1 (thick solid lines) and the Model 2 (thin dashed lines) in Case 11.

optimum values of C_{br} and K (Eq.(16)) are determined in the calibrations for the Model 2. The coefficients were varied as follows:

$$\begin{aligned} C_{br} &= 0.8 + 0.05\,(k_2 - 1), & k_2 &= 1,2,....,6, \\ C_B &= 0.5 + 0.1\,(k_3 - 1), & k_3 &= 1,2,....,8, \\ K &= 0.025 k_4, & k_4 &= 1,2,....,8. \end{aligned} \tag{19}$$

For determining the optimum coefficients that minimize error, a single error index is used for evaluating errors in $H_{1/3}$ and Q_b. The following procedure is used to calculate the error index for the Model 1.

1) The error of $H_{1/3}$ predicted with k_2-th C_{br} and k_3-th C_B in Case k_1, denoted as $(E_H)_{k_1,k_2,k_3}$, and that of Q_b, denoted as $(E_Q)_{k_1,k_2,k_3}$, are given by

$$\begin{aligned} (E_H)_{k_1,k_2,k_3} &= \sqrt{\frac{\sum_{n=1}^{N_{H,k_1}} \left\{(H_{1/3,p})_n - (H_{1/3,m})_n\right\}^2}{N_{H,k_1}}}, \\ (E_Q)_{k_1,k_2,k_3} &= \sqrt{\frac{\sum_{n=1}^{N_{Q,k_1}} \left\{(Q_{b,p})_n - (Q_{b,m})_n\right\}^2}{N_{Q,k_1}}}, \end{aligned} \tag{20}$$

where the values of $N_{H,k1}$ and $N_{Q,k1}$ are the numbers of measured values for $H_{1/3}$ and Q_b.

2) The mean error in $H_{1/3}$ for all cases, denoted as $(E_H)_{k_2,k_3}$, and that in Q_b, denoted as $(E_Q)_{k_2,k_3}$, are given by

$$\begin{aligned} (E_H)_{k_2,k_3} &= \frac{\sum_{k_1=1}^{11} (E_H)_{k_1,k_2,k_3}}{11}, \\ (E_Q)_{k_2,k_3} &= \frac{\sum_{k_1=1}^{11} (E_Q)_{k_1,k_2,k_3}}{11}. \end{aligned} \tag{21}$$

Then, the mean and the standard deviation of $(E_H)_{k_2,k_3}$ for all values of C_{br} and C_B, denoted as $\overline{E_H}$ and S_H, and those of $(E_Q)_{k_2,k_3}$, denoted as $\overline{E_Q}$ and S_Q, are estimated by

$$\begin{aligned} \overline{E_H} &= \sum_{k_3=1}^{8} \sum_{k_2=1}^{6} (E_H)_{k_2,k_3} / 48, \\ S_H &= \sqrt{\sum_{k_3=1}^{8} \sum_{k_2=1}^{6} \left\{(E_H)_{k_2,k_3} - \overline{E_H}\right\}^2 / 48}, \\ \overline{E_Q} &= \sum_{k_3=1}^{8} \sum_{k_2=1}^{6} (E_Q)_{k_2,k_3} / 48, \\ S_Q &= \sqrt{\sum_{k_3=1}^{8} \sum_{k_2=1}^{6} \left\{(E_Q)_{k_2,k_3} - \overline{E_Q}\right\}^2 / 48}. \end{aligned} \tag{22}$$

3) Finally, the error index at the k_2-th C_{br} and the k_3-th C_B is given by

$$E_{k_2,k_3} = \frac{(E_H)_{k_2,k_3} - \overline{E_H}}{S_H} + \frac{(E_Q)_{k_2,k_3} - \overline{E_Q}}{S_Q}. \tag{23}$$

In the calibrations for the Model 2, C_{br} and K are varied, and the error index is similarly estimated by Eqs.(20) - (23) where k_3 is replaced by k_4.

Figures 12 (1) and **(2)** show contour plots of E, estimated by Eq.(23), for the Model 1 and the Model 2. The optimum values of the coefficients are found to be $C_{br} = 0.95$ and $C_B = 0.8$ in the Model 1, and $C_{br} = 0.95$ and $K = 0.075$ in the Model 2.

The comparisons of $H_{1/3}$ and Q_b measured in the field and those estimated by the Model 1 and the Model

2 containing the new coefficients, calibrated with the field data, are shown in **Figures 13 (1) - (11)**. **Tables 4 (1)** and **(2)** list E_H and E_Q, estimated by Eq.(20), for the Model 1 and the Model 2 both containing the old coefficients, calibrated with experimental data, and the new coefficients. The shortcomings of the models containing the old coefficients are improved; the accuracy of Q_b estimated with the new coefficients increases though that of $H_{1/3}$ slightly decreases. The values of Q_b estimated by the models containing the new coefficients, except for those in the Case 3, agree with the field data on the longshore bars as well as on the troughs. In the Case 3, wave breaking was poorly reproduced by the Model 1 and also by the Model 2. As a result, Q_b and $H_{1/3}$ in the Case 3 estimated by the models disagree with the field data.

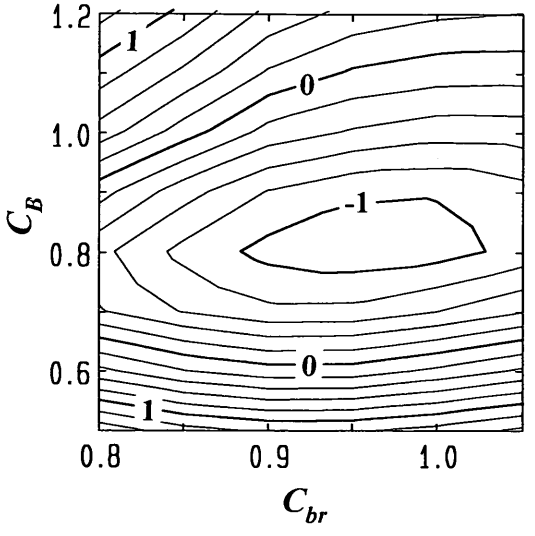

Figure 12 (1) Contour plot of E, estimated by Eq.(23), for the Model 1.

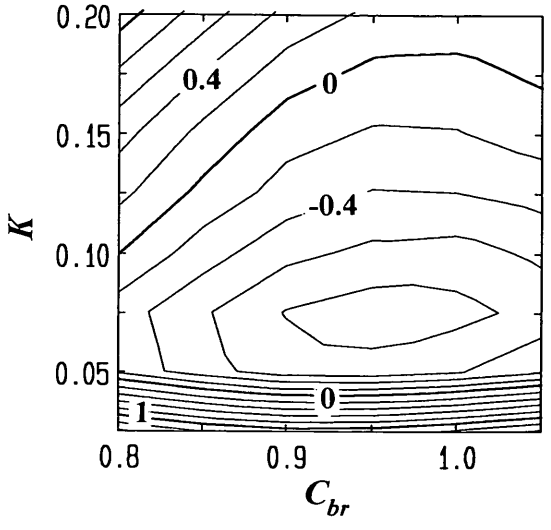

Figure 12 (2) Contour plot of E, estimated by Eq.(23), for the Model 2.

Table 4 (1) The values of E_H and E_Q for the Model 1

Case	Model 1			
	Old Coefficient		New Coefficient	
	E_H (m)	E_Q	E_H (m)	E_Q
1	0.17	0.18	0.14	0.13
2	0.27	0.20	0.21	0.13
3	0.16	0.20	0.18	0.20
4	0.12	0.14	0.11	0.12
5	0.16	0.12	0.12	0.08
6	0.09	0.10	0.15	0.06
7	0.08	0.14	0.20	0.08
8	0.14	0.22	0.15	0.10
9	0.11	0.14	0.29	0.10
10	0.17	0.24	0.24	0.17
11	0.18	0.16	0.12	0.11
Mean	0.15	0.17	0.17	0.12

Table 4 (2) The values of E_H and E_Q for the Model 2

Case	Model 2			
	Old Coefficient		New Coefficient	
	E_H (m)	E_Q	E_H (m)	E_Q
1	0.14	0.15	0.11	0.13
2	0.26	0.17	0.21	0.14
3	0.16	0.20	0.17	0.20
4	0.15	0.14	0.12	0.13
5	0.17	0.12	0.11	0.11
6	0.11	0.10	0.13	0.09
7	0.08	0.19	0.16	0.09
8	0.14	0.24	0.12	0.15
9	0.15	0.16	0.29	0.10
10	0.16	0.26	0.22	0.17
11	0.15	0.17	0.13	0.11
Mean	0.15	0.17	0.16	0.13

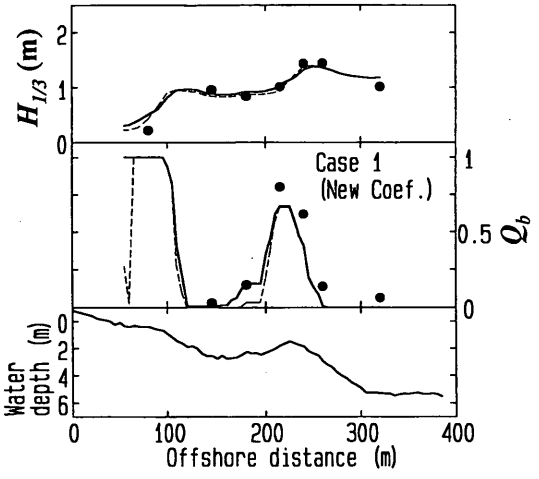

Figure 13 (1) Comparison of $H_{1/3}$ and Q_b measured in the field (solid circles) and those estimated by the Model 1 (thick solid lines) and the Model 2 (thin dashed lines) with new coefficients, calibrated with field data, in Case 1.

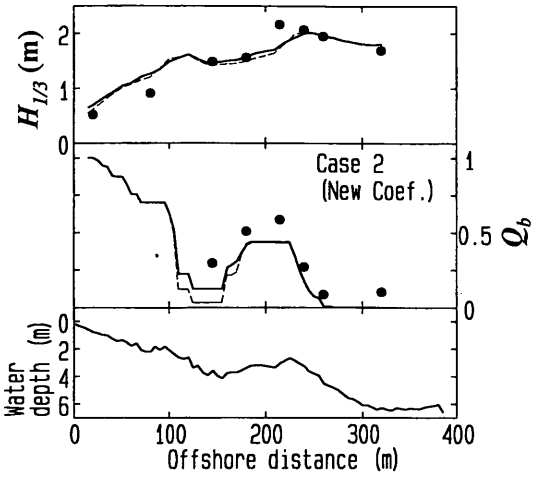

Figure 13 (2) Comparison of $H_{1/3}$ and Q_b measured in the field (solid circles) and those estimated by the Model 1 (thick solid lines) and the Model 2 (thin dashed lines) with new coefficients, calibrated with field data, in Case 2.

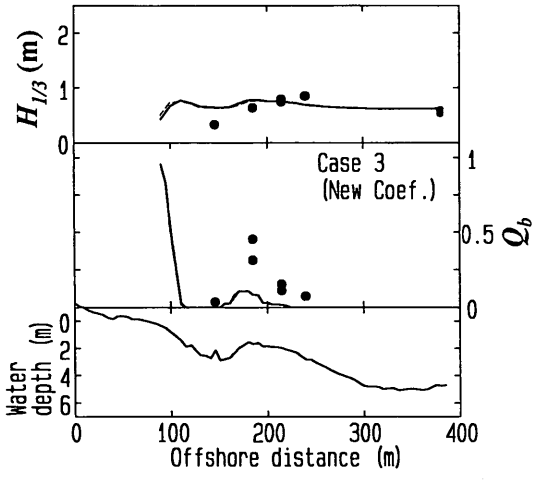

Figure 13 (3) Comparison of $H_{1/3}$ and Q_b measured in the field (solid circles) and those estimated by the Model 1 (thick solid lines) and the Model 2 (thin dashed lines) with new coefficients, calibrated with field data, in Case 3.

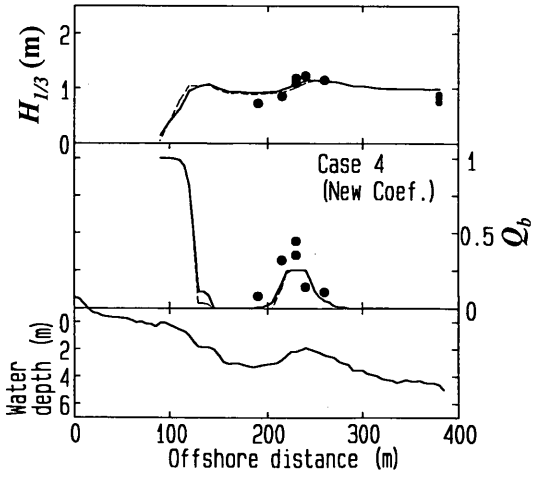

Figure 13 (4) Comparison of $H_{1/3}$ and Q_b measured in the field (solid circles) and those estimated by the Model 1 (thick solid lines) and the Model 2 (thin dashed lines) with new coefficients, calibrated with field data, in Case 4.

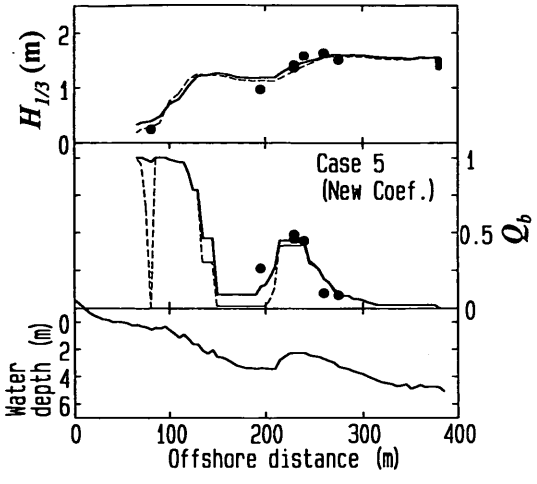

Figure 13 (5) Comparison of $H_{1/3}$ and Q_b measured in the field (solid circles) and those estimated by the Model 1 (thick solid lines) and the Model 2 (thin dashed lines) with new coefficients, calibrated with field data, in Case 5.

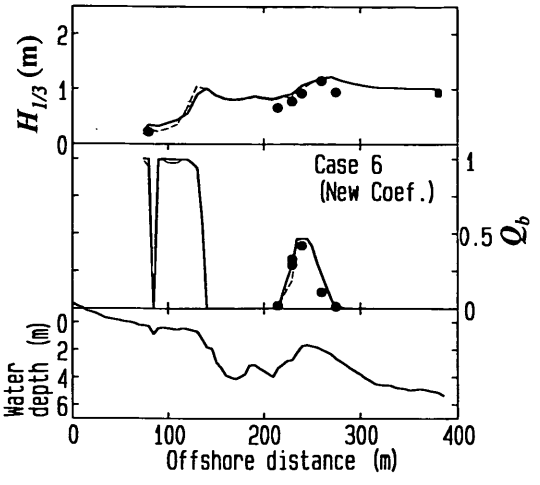

Figure 13 (6) Comparison of $H_{1/3}$ and Q_b measured in the field (solid circles) and those estimated by the Model 1 (thick solid lines) and the Model 2 (thin dashed lines) with new coefficients, calibrated with field data, in Case 6.

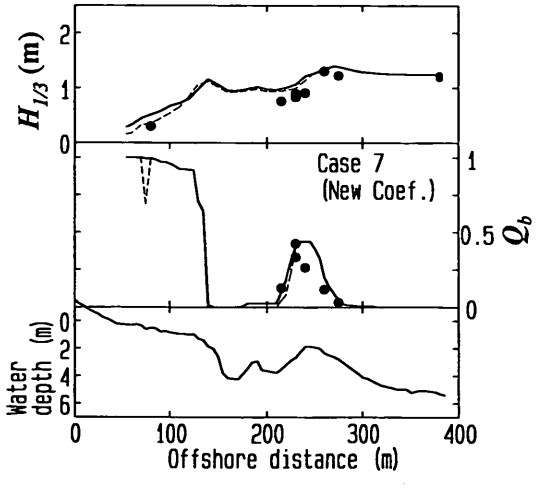

Figure 13 (7) Comparison of $H_{1/3}$ and Q_b measured in the field (solid circles) and those estimated by the Model 1 (thick solid lines) and the Model 2 (thin dashed lines) with new coefficients, calibrated with field data, in Case 7.

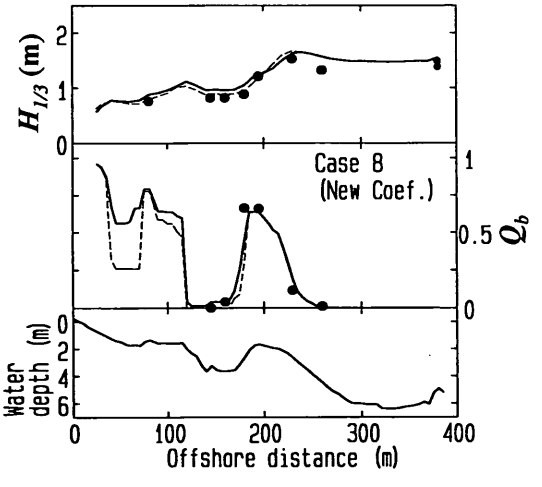

Figure 13 (8) Comparison of $H_{1/3}$ and Q_b measured in the field (solid circles) and those estimated by the Model 1 (thick solid lines) and the Model 2 (thin dashed lines) with new coefficients, calibrated with field data, in Case 8.

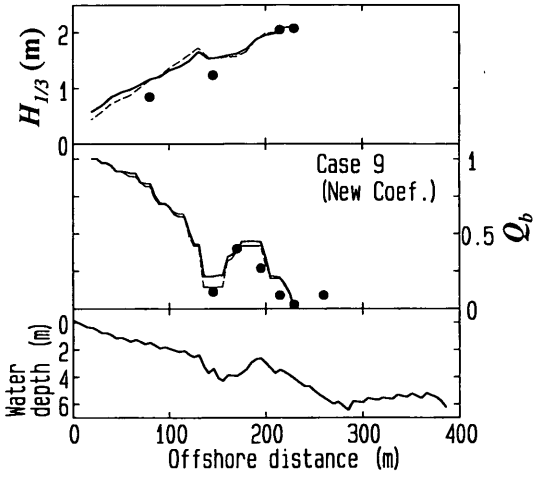

Figure 13 (9) Comparison of $H_{1/3}$ and Q_b measured in the field (solid circles) and those estimated by the Model 1 (thick solid lines) and the Model 2 (thin dashed lines) with new coefficients, calibrated with field data, in Case 9.

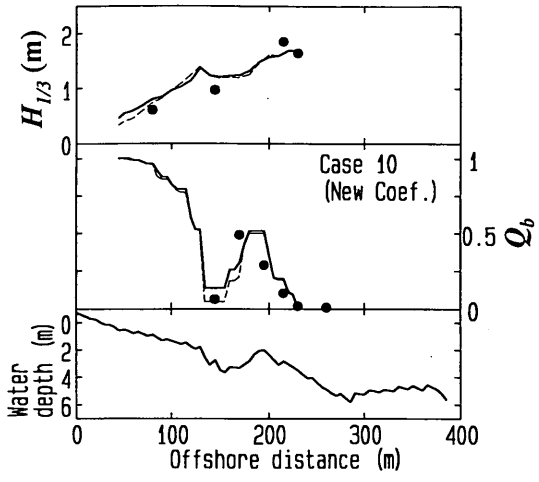

Figure 13 (10) Comparison of $H_{1/3}$ and Q_b measured in the field (solid circles) and those estimated by the Model 1 (thick solid lines) and the Model 2 (thin dashed lines) with new coefficients, calibrated with field data, in Case 10.

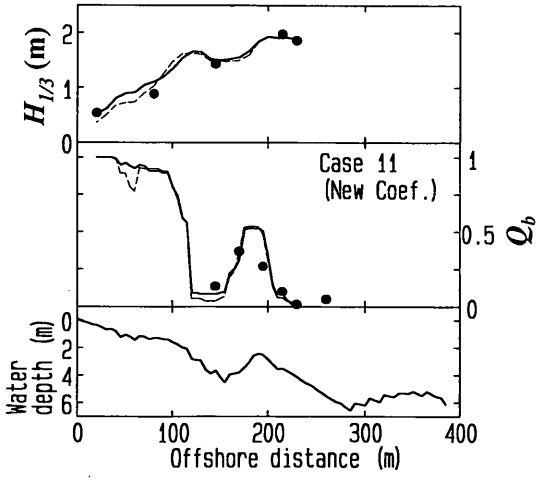

Figure 13 (11) Comparison of $H_{1/3}$ and Q_b measured in the field (solid circles) and those estimated by the Model 1 (thick solid lines) and the Model 2 (thin dashed lines) with new coefficients, calibrated with field data, in Case 11.

Although the differences between Q_b estimated by the Model 1 and those by the Model 2 are small, Q_b estimated by the Model 2 more decrease at the troughs toward the shore and are more sensitive to the change in water depth near the shorelines than those estimated by the Model 1.

5.3 Verification

The models are compared with large-scale experiment data of the Delta Flume '93 Experiments (*Rivero et al.*, 1994). The data shown by *Rivero et al.* (1994) are Q_b and H_{m0}, defined as

$$H_{m0} = 4.004\eta_{rms}. \tag{24}$$

The present models cannot predict H_{m0} because H_{m0} is estimated from a series of water surface elevation, which the present models cannot predict. For comparing the present models with the large-scale experiments, a certain relation between η_{rms} and $H_{1/3}$ is required.

Outside the surf zone, using field data, *Goda* (1983) has investigated the relation between $H_{1/3}/\eta_{rms}$ and a wave nonlinearity parameter $\pi_{1/3}$, which is defined as

$$\pi_{1/3} = \frac{H_{1/3}}{L}\left(\tanh\frac{2\pi h}{L}\right)^{-3}, \tag{25}$$

where L is the wavelength at the water depth of h. *Goda* (1983) reported that $H_{1/3}/\eta_{rms}$ increases with the increase of $\pi_{1/3}$ when $\pi_{1/3} \geq 0.1$, while $H_{1/3}/\eta_{rms}$ is constant and about 3.8 when $\pi_{1/3} < 0.1$.

Although the relation between $H_{1/3}$ and η_{rms} out of the surf zone was investigated, no relation between $H_{1/3}$ and η_{rms} in the surf zone was reported. We hence investigate the relation with the field data of the eleven cases. The relation is shown in **Figure 14**, where the solid line shows the relation obtained with the method of least squares, and the dashed line shows $H_{1/3}/\eta_{rms}$ =3.8. The value of $H_{1/3}/\eta_{rms}$ in the surf zone increases with the increase of $\pi_{1/3}$ when $\pi_{1/3} \geq 0.1$, while $H_{1/3}/\eta_{rms}$ is about 3.8 when $\pi_{1/3} < 0.1$. Thus we assume that

$$\begin{aligned} H_{1/3}/\eta_{rms} &= 0.349 \ln \pi_{1/3} + 4.648, \quad \pi_{1/3} \geq 0.1, \\ H_{1/3}/\eta_{rms} &= 3.8, \qquad\qquad\quad \pi_{1/3} < 0.1. \end{aligned} \tag{26}$$

The upper equation of Eq.(26) is the relation obtained with the method of least squares.

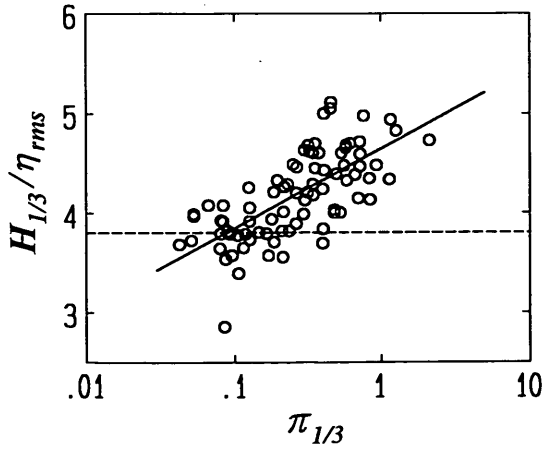

Figure 14 Relation of $H_{1/3}/\eta_{rms}$ and $\pi_{1/3}$.

With the relation expressed as Eq.(26), $H_{1/3}$ predicted by the Model 1 and Model 2 are translated to H_{m0}, and the translated H_{m0} and the predicted Q_b are compared with the values measured in cases 1A, 1B, and 1C of the Delta Flume '93 Experiment (*Rivero et al.*, 1994). The comparisons are shown in **Figures 15 (1) - (3)**. In all cases, the values of H_{m0} predicted by the Model 1 are almost equal to those predicted by the Model 2, and both values agree with the measured values quite well. Hence, the discussion is focused on the fraction of breaking waves. On the planar beach for the case of 1A, the predicted Q_b agree with the measured values though the predicted values are smaller than the measured ones. On a barred beach for the case of 1B, Q_b predicted at the trough do not decrease toward the shore, and agree with the measured values, while the present models overestimate Q_b out of the trough. On another barred beach for the case of 1C, although the predicted Q_b slightly decrease toward the shore at the trough, the predicted Q_b agree with the measured values. Out of the trough, the present models also overestimated Q_b. Compared with Q_b predicted by *Southgate and Wallace* (1994) for the cases of 1A, 1B and 1C, Q_b predicted by the present models are not sensitive to the change in water depth at the troughs, and Q_b variations predicted by the present models are smooth.

6. Discussion

The models developed in this study include the wave reforming criterion proposed on the basis of field data and the coefficients calibrated with the field data. Through the investigation on wave reforming and the calibrations of the models, scale effects are recognized in the following quantities: H_b/h_b, the rate of wave energy dissipation due to wave breaking and H_r/h_r. The values of H_r/h_r in the field are smaller than those in a small- scale experiment, while H_b/h_b and the energy dissipation in the field seem to be smaller than those in small scale experiments.

Although a cause of the scale effect in H_b/h_b is unknown, we think the scale effects in H_r/h_r and wave energy dissipation are due to the size of vortex and turbulence generated by wave breaking. The difference of the size of the vortex and turbulence probably results in the difference of the energy dissipation process and different H_r/h_r.

Whereas we recognized scale effect in wave energy dissipation due to wave breaking, which influences strongly the wave height variation in the surf zone, *Stive* (1985) reported that scale effect in wave height variation in the surf zone was negligible by comparing wave height variations in different scales on planar beaches. On a planar beach, waves continuously break and few waves reform. On the other hand, at a trough on a barred beach, few waves newly break and some waves reform. The difference of the wave condition seems to result in the difference of the appearance of scale effect.

Because scale effects are recognized in H_b/h_b, H_r/h_r, and energy dissipation rate, the scale effects must be included in the present models; for example, coefficients in the present models should be functions of a scale such as wave height. The scale effects, however, are not considered in the present models. Accordingly, the models are thought to be applied only to waves whose heights range from 0.5 m to 2.0 m, where the waves for the calibrations are included.

Models employing the wave-by-wave approach like the Model 1 and the Model 2 have a serious limitation; the models cannot predict the change in wave period due to wave decomposition because the models assume the numbers of waves are constant. The wave decomposition frequently occurs over longshore bars, and results in the decrease of wave period. Future improvement of the models are required.

In the chapter 3, the correlation between A and $(h_{trg} - h_{bar})/h_{bar}$ is found; that is, A increase as $(h_{trg} - h_{bar})/h_{bar}$ increase. Two causes of the correlation are thought.

1) When $h_{trg} - h_{bar}$ is large, the increase of H_r at a trough toward the shore is large. The large increase of H_r

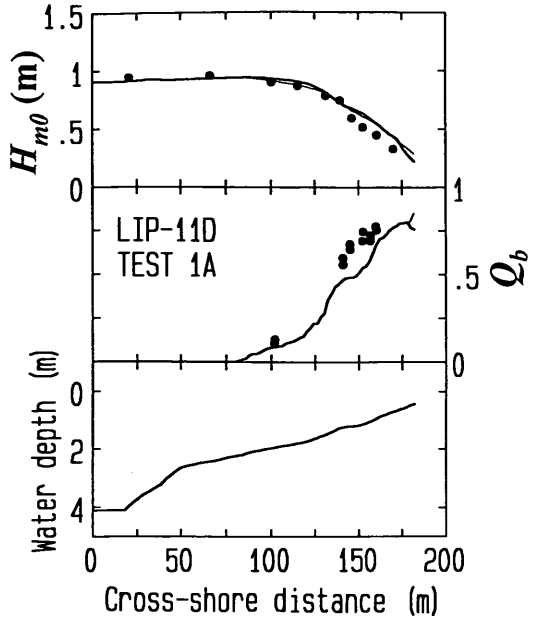

Figure 15 (1) Comparison of H_{m0} and Q_b measured in a large scale experiment (solid circles) and those estimated by the Model 1 (thick solid lines) and the Model 2 (thin dashed lines) in Case 1A.

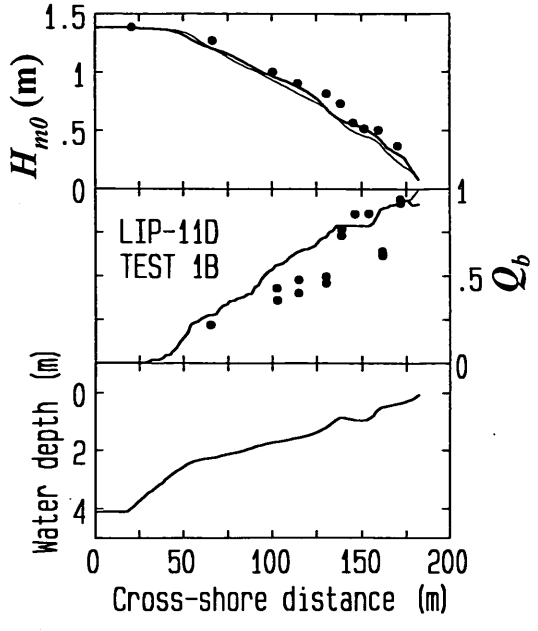

Figure 15 (2) Comparison of H_{m0} and Q_b measured in a large scale experiment (solid circles) and those estimated by the Model 1 (thick solid lines) and the Model 2 (thin dashed lines) in Case 1B.

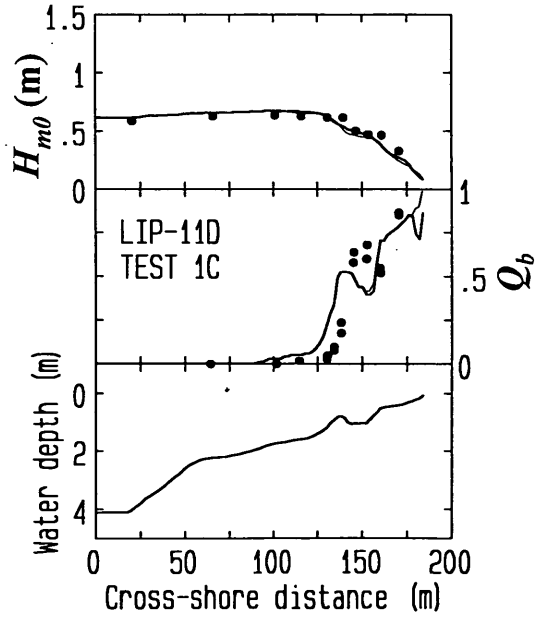

Figure 15 (3) Comparison of H_{m0} and Q_b measured in a large scale experiment (solid circles) and those estimated by the Model 1 (thick solid lines) and the Model 2 (thin dashed lines) in Case 1C.

makes more broken waves reform than a small increase of H_r, and results in a sharp decrease of Q_b.
2) When h_{bar} is small, H_b is small; the small H_b makes more waves break than a large H_b. Furthermore, the small h_{bar} results in the small difference between H_b and H_r. **Figure 16 (1)** and **(2)** show examples of the relation between H_b - H_r and h/L_0; H_b and H_r are estimated by Eq.(10) and Eq.(9). The value of H_b - H_r decreases with the decrease of h. When H_b - H_r is small, broken waves reform with small energy dissipation. As a result, the decrease of Q_b becomes sharp.

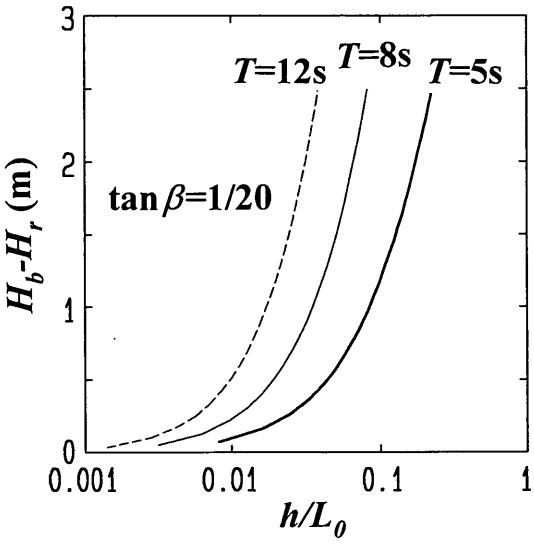

Figure 16 (1) The values of H_b - H_r as a function of h/L_0 at tan β =1/20.

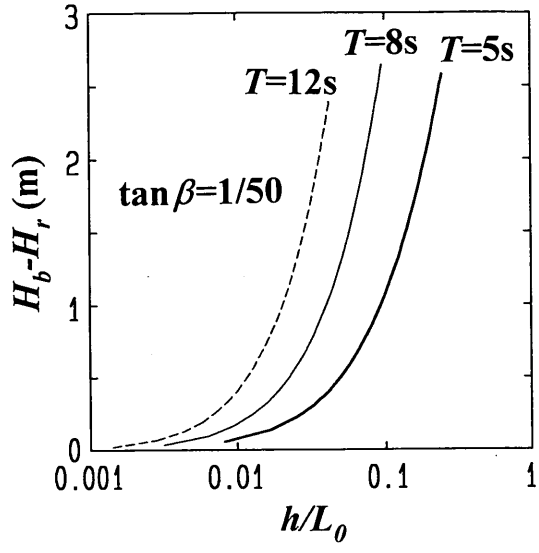

Figure 16 (2) The values of H_b - H_r as a function of h/L_0 at tan β =1/50.

Figures 17 (1) and **(2)** are examples indicating that the item 2) is a cause of the correlation between A and $(h_{trg} - h_{bar})/h_{bar}$. The figures show the wave height distributions from P240m to P180m in Cases 1 and 2; the crests of the longshore bars were located at P225m in both Cases, and h_{bar} = 1.49 m in Case 1 and h_{bar} = 2.70 m in Case 2. The wave height distributions of broken waves are indicated by the bars with slashed lines and those of all waves are indicated by the open bars. The solid lines with arrows indicate H_r estimated by Eq.(9) using the mean wave periods. The dashed lines with arrows at P240m indicate H_b estimated by Eq.(10) using the mean wave periods, while the dashed lines at P215m and P180m indicate H_b at the bar crests, P225m.

In Case 1, because H_b - H_r was small, a broken wave reformed with small energy dissipation. As a result, almost all broken waves reformed up to P180m. On the other hand, in Case 2, some waves were still broken even at P180m owing to the large H_b - H_r. As a result, the decrease of Q_b shoreward of the bar crest in Case 2 was smaller than that in Case 1.

In the chapter 4, the measured cross-shore wind velocities, which ranged from -8.0 m/s to 2.8 m/s, were proved to have little influence on H_r/h_r. The influence of wind on wave breaking, however, is found in the field by *Galloway et al.* (1989) and *Dally* (1992). Thus, probably wind has some effect on H_r/h_r. The relation between wind velocity and H_r/h_r should be investigated again with data including a wide range of wind velocities.

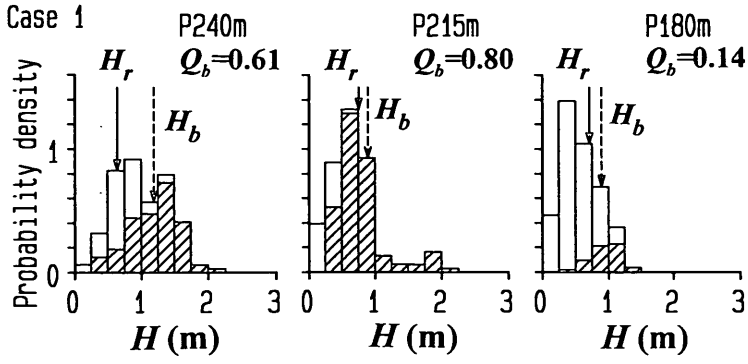

Figure 17 (1) Wave height distributions and broken wave height distributions (dashed area) in Case 1.

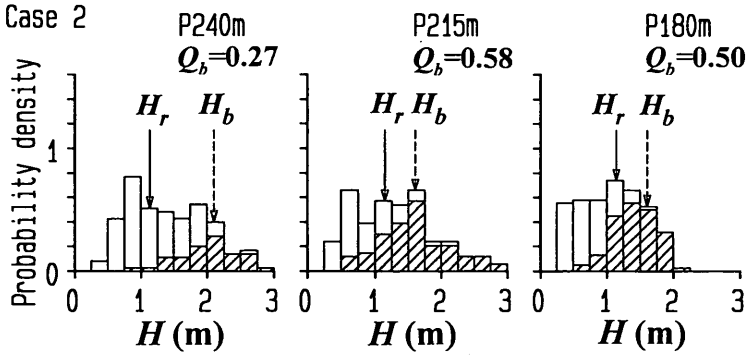

Figure 17 (2) Wave height distributions and broken wave height distributions (dashed area) in Case 2.

7. Summary and Conclusions

Field measurements of wave height and the fraction of breaking waves on longshore bars and troughs were carried out at Hazaki Oceanographical Research Station (HORS). Water surface elevations were measured with ultrasonic wave gages, and modes of wave breaking, breaking or broken or non-breaking, were visually observed. Shoreward of a bar crest, the decrease of the fraction of breaking waves Q_b toward the shore depended on the water depth at the bar crest h_{bar} and that at the trough h_{trg}; that is, the decrease rate of Q_b increased as $(h_{trg}-h_{bar})/h_{bar}$ increased.

The wave height-water depth ratio at wave reforming H_r/h_r was investigated with field data obtained at the troughs. The values of H_r/h_r decreased as the wave periods decreased, and the relation between H_r/h_r and h_r/L_0 was expressed as Eq.(9). Most H_r/h_r in the field were smaller than those in a small-scale experiment.

Models for $H_{1/3}$ and Q_b employing the wave-by-wave approach were developed. The performances of the models containing sub-models for wave breaking and energy dissipation calibrated with experimental data were not satisfied; Q_b estimated by the models were smaller than those measured on the troughs. New coefficients were therefore introduced, and the models were calibrated with the field data. The models calibrated with the field data predicted $H_{1/3}$ and Q_b well on the longshore bars as well as on the troughs. The validity of the models was also verified with large-scale experiment data.

Acknowledgements

We are grateful to the following research engineers for their great contributions on the field measurements, which required patience in particular in winter: Messrs. Satoshi Nakamura and Masato Fukuda, a member and a former member of the Port and Harbour Research Institute (PHRI). We would also like to thank Drs. Takeshi Horie and Hiroaki Ozasa, the Deputy Director General of PHRI and the Director of Marine Environment Division, PHRI, for their valuable suggestions concerning the manuscript. The offshore wave data were provided by Kashima Port Construction Office of the Second District Port Construction Bureau, Ministry of Transport, and the Marine Observation Laboratory of PHRI. Further acknowledgement is extended to Dr. Kazumasa Katoh, the Chief of the Littoral Drift Laboratory of PHRI for his critical review and useful comments that improved this paper.

(Received on November 30, 1995)

References

Battjes J.A. and J.P.F.M. Janssen (1978) : Energy loss and set-up due to breaking of random waves, *Proc. 16th Coastal Eng. Conf.*, ASCE, pp.569-587.

Battjes J.A. and M.J.F. Stive (1985) : Calibration and verification of a dissipation model for random breaking waves, *J. Geophys. Res.*, Vol.90, No.C5, pp.9159-9167.

Dally W.R., R.G. Dean and R.A. Dalrymple (1985) : Wave height variation across beaches of arbitrary profile, *J. Geophys. Res.*, Vol.90, No.C6, pp.11,917-11,927.

Dally W.R. (1992) : Random breaking waves: field verification of a wave- by-wave algorithm for engineering application, *Coastal Eng.*, 16, pp.369-397.

Ebersole B.A. (1987) : Measurement and prediction of wave height decay in the surf zone. *Coastal Hydrodynamics*, ASCE, pp.1-16.

Galloway J.S., M.B. Collins and A.D. Moran (1989) : Onshore/offshore wind influence on breaking waves: an empirical study, *Coastal Eng.*, 13, pp.305-323.

Goda Y.(1983) : A unified nonlinearity parameter of water waves, *Rep. Port and Harbour Res. Inst.*, Vol.22, No.3, pp.3-30.

Hashimoto N., T. Nagai and T. Asai (1994) : Extension of the maximum entropy principle method for directional wave spectrum estimation, *Proc. 24th Coastal Eng. Conf.*, ASCE, pp.232-246.

Horikawa K. and C.T. Kuo (1966) : A study on wave transformation inside surf zone, *Proc. 10th Coastal Eng. Conf.*, ASCE, pp.217-233.

Hotta S. and M. Mizuguchi (1980) : A field study of waves in the surf zone, *Coastal Eng. Japan*, Vol.23, pp.59-79.

Kuriyama Y. (1994) : Numerical model for longshore current distribution on a bar-trough beach, *Proc. 24th Coastal Eng. Conf.*, ASCE, pp.2237-2251.

Kweon H.M. and Y. Goda (1994) : The study of energy dissipation of regular wave on the arbitrary profile, *Proc. Civil Eng. in Ocean*, Vol.10, JSCE, pp.31-36. (in Japanese)

Nishi R. (1994) : Probability of wave breaking on a plane beach, *Proc. of International Symposium: Waves-Physical and Numerical Modelling*, pp.773-782.

Rivero F.J., A.S. Arcilla and D. Beyer (1994) : Comparison of a wave transformation model with LIP-11D data, *Coastal Dynamics '94*, ASCE, pp.518-532.

Roelvink J.A. (1993) : Dissipation in random wave groups incident on a beach, *Coastal Eng.*, 19, pp.127-150.

Seyama A. and A. Kimura (1988) : The measured properties of irregular wave breaking and wave height

change after breaking on the slope, *Proc. 21st Coastal Eng. Conf.*, ASCE, pp.419-432.
Shuto N. (1974): Nonlinear long waves in a channel of variable section, *Coastal Eng. Japan*, Vol.17, pp.1-12.
Southgate H.N. and R.B. Nairn (1993): Deterministic profile modelling of nearshore processes. Part1. waves and currents, *Coastal Eng.*, 19, pp.27-56.
Southgate H.N. and H.M. Wallace (1994) : Breaking wave persistence in parametric surf zone models, *Coastal Dynamics '94*, ASCE, pp.543-555.
Stive M.J.F. (1985) : A scale comparison of waves breaking on a beach, *Coastal Eng.*, 9, pp.151-158.
Thornton E.B. and R.T. Guza (1982) : Energy saturation and phase speeds measured on a natural beach, *J. Geophys. Res.*, Vol.87, No.C12, pp.9499-9508.
Thornton E.B. and R.T. Guza (1983) : Transformation of wave height distribution, *J. Geophys. Res.*, Vol.88, No.C10, pp.5925-5938.
Whitford D.J. and E.B. Thornton (1988) : Longshore current forcing at a barred beach, *Proc. 21st Coastal Eng. Conf.*, ASCE, pp.77-90.

List of Main Symbols

A : dissipation coefficient in Eq.(3)
AIC : Akaike's Information Criterion estimated by Eq.(4)
B : dimensionless coefficient in Eq.(12)
C_B: dimensionless coefficient in Eq.(18)
C_{br}: dimensionless coefficient in Eq.(17)
C_g: group velocity
E : error index estimated by Eq.(23)
E_w: wave energy
g : gravity acceleration
H_b: breaking wave height
H_m: mean wave height
H_{m0}: wave height defined as Eq.(24)
H_{rms}: root-mean-square wave height
H_r: wave height at wave reforming
H_S: stable wave height
$H_{1/3}$: the significant wave height
$(H_{1/3})_0$: the significant wave height in deep water
h : water depth
h_b: breaking water depth
h_{bar}: water depth at a bar crest
h_r: water depth at wave reforming
h_{trg}: water depth at a trough
K : dimensionless coefficient in Eq.(16)
L_0: wavelength in deep water
l : the length of a region defined as Eq.(15)
M_A: the number of free parameters contained in a model
N_A: the number of data points
Q_b: the fraction of breaking waves
$(Q_b)_{bar}$: the fraction of breaking waves at a bar crest

$(Q_b)_{skb}$: the fraction of breaking waves shoreward of a bar crest
$\tan\beta$: beach slope
T_l: the period when a wave having the mean wave period travels from a seaward measurement point to the shoreward measurement point
$T_{1/3}$: the significant wave period
$(T_{1/3})_0$: the significant wave period in deep water
W_b: the band width used in the analysis of water surface elevation data
W_c: cross-shore wind velocity
W_l: longshore wind velocity
x: offshore distance
x_{bar}: offshore distance at a bar crest
Γ: dimensionless coefficient in Eq.(16)
δ: standard deviation of H_b/h_b
η_i: the i-th water surface elevation
θ_b: wave direction visually observed at a bar crest
$\pi_{1/3}$: wave nonlinearity parameter defined as Eq.(25)
ρ: density of sea water